Stockholm University

Bachelor Thesis

Degree Project in Geology 15 hp

Petrological study of the transition from high pressure to low pressure rocks on Syros, Greece

Carolina Månbro

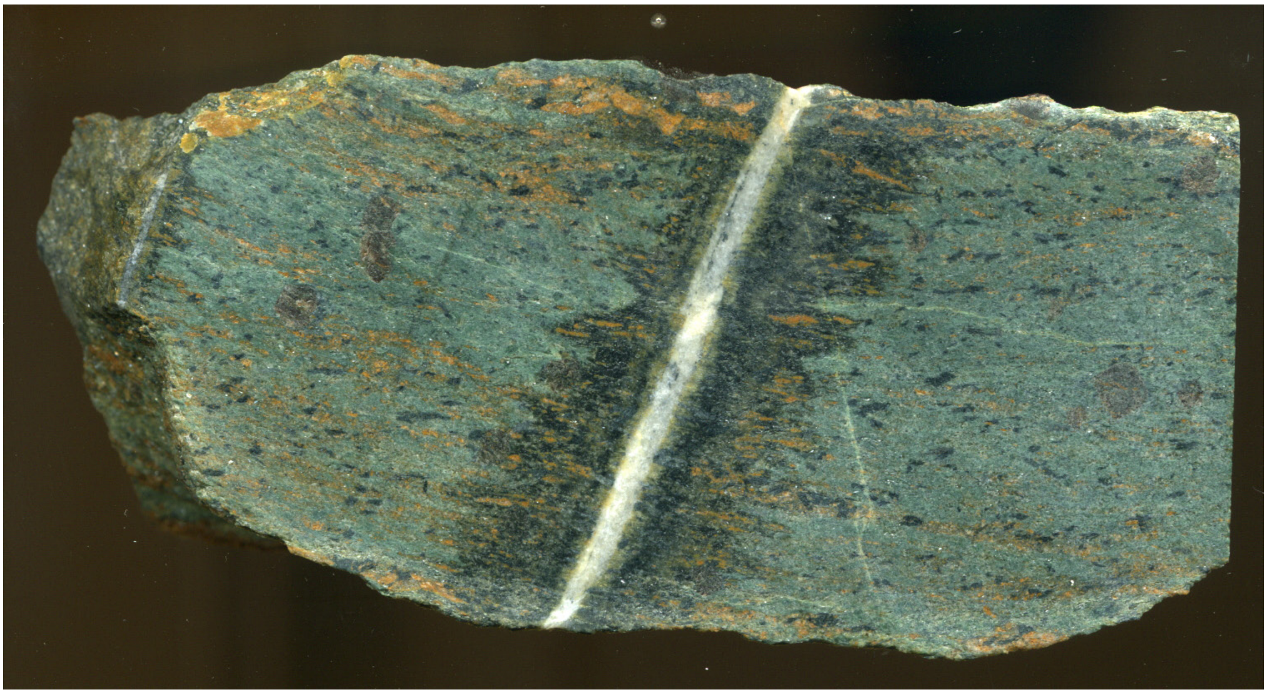

Stockholm 2018

Department of Geological Sciences
Stockholm University
SE-106 91 Stockholm
Sweden

Abstract

Veins with alteration haloes can be seen cross-cutting well-preserved eclogite facies meta-basalts on the island of Syros, Greece.

Thin section analysis of the samples collected reveals that the alteration haloes are the result of two individual vein forming events, occurring under different P-T conditions. The first veining event took place under blueschist facies conditions, where the eclogite meta-basalt acted in a brittle-ductile manner, altering the selvages of the veins to a blueschist facies mineral assemblage. The second vein forming event occurred under greenschist facies conditions, where the eclogite meta-basalts acted in a brittle manner, retrogressing both the eclogite rocks in the selvages of the newly formed veins, as well as some of the older blueschist facies haloes already present, to a greenschist facies mineral assemblage.

The fluids present in the veins at the time of the greenschist facies event shows indications of being of two different compositions. Fluids with higher X_{CO2} seems to have been present in some of the veins, stabilizing the blueschist facies minerals in the haloes of these veins, while the veins containing fluids with a lower X_{CO2} developed greenschist facies haloes.

Innehåll

Introduction

High pressure-low temperature (HP-LT) rocks are formed by rapid subduction at convergent plate boundaries. Rapid subduction combined with the slow thermal conductivity of rocks causes the minerals in the subducting slab to be subjected to high pressure regimes, while the temperature increase is moderate. The increase in pressure causes dehydration and increased density of the mineralogy in the subducting slab (Manea *et al.*, 2004; Palin *et al.*, 2016), which results in the formation of HP-LT mineral assemblages of the blueschist and eclogite facies (fig. 1). These HP-LT mineral assemblages are often subjected to metamorphic fluid flow and a higher thermal regime during their return to the surface, causing overprinting/re-equilibration at granulite, amphibolite and/or greenschist facies conditions (Ernst, 2006) (fig. 1).

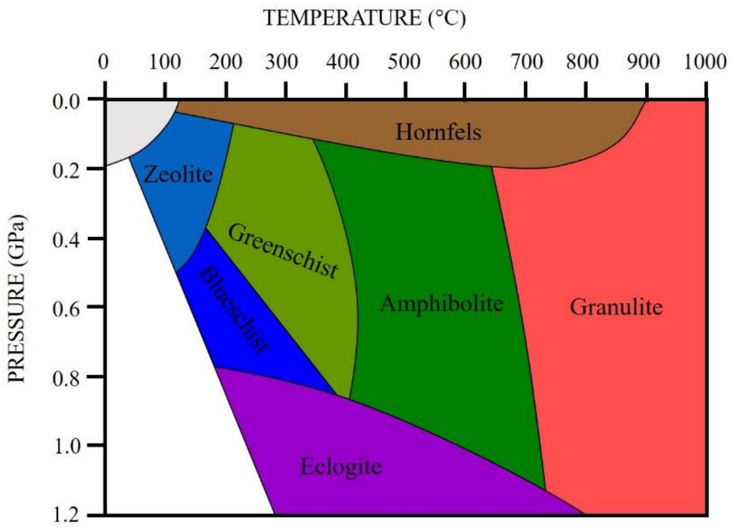

Fig. 1: Metamorphic facies diagram after Eskola (1915).

There are only a few places in the world where HP-LT rocks have been exhumed to the surface without mineral replacement at lower-P and/or higher-T conditions. The exact processes behind this type of exhumation is debated (Jolivet & Brun, 2008), but there is a general consensus that rapid exhumation is a key factor. Rapid exhumation in a (near to) isothermal regime is a result from tectonic forces, e.g. thrust faulting (Ring & Glodny, 2010) or rapid extension (Ernst, 2006), possibly in combination with denudation on a larger scale (Ring *et al*., 1999; Ernst 2006). This causes rapid exhumation of the underlying rocks, and preserves the HP-LT rocks as metastable at the Earth's surface.

There have been some studies though that have shown that exhumation does not necessarily need to have been rapid if fluids are absent (Schliestedt & Matthews, 1987; Barrientos & Selverstone, 1993) or if a fluid of a composition that stabilizes HP-LT minerals is present during exhumation (Bröcker, 1990; Kleine *et al*., 2014).

The need for fluids to be present in order to retrogress eclogite- and blueschist facies rocks, to that of a lower grade mineral assemblage (e.g. greenschist facies), is supported by the reactions in which the HP-LT minerals are altered. The minerals of the lower grade facies contains more $H_2O \pm CO_2$ than does the HP-LT minerals (Etheridge *et al.*, 1983; Schliestedt & Matthews, 1987; Barrientos & Selverstone, 1993), thus, for these retrograde rehydration reactions to occur, the introduction of a fluid is essential. The alteration of rocks due to fluid infiltration (hydration) and by chemical exchange between minerals and (in HP-LT rocks usually metamorphic) fluids (metasomatism) are well-known processes that are very common in retrograde metamorphism. Fluid-infiltration with hydration, and possibly metasomatism, as a result can occur both on a regional scale as well as on a local scale. Fluid-rock interaction over larger areas is the result of a high volume of fluids, usually in combination with more permeable rocks (Etheridge *et al.*, 1983). This causes fluid flow to be more pervasive, resulting in widespread re-equilibration of the rock volume at the pressure-temperature (P-T) conditions at the time of infiltration.

Large scale re-equilibration does not always occur since there are different mechanisms that can lead to fluid flow not being pervasive throughout the rock. These can be 1) low permeability rock volumes, 2) impermeable rock layers “shielding” the surrounding rocks from the fluids, 3) the fluids being highly channelized via weaknesses in the rock, e.g. shear zones, bedding planes, foliation planes and veins, 4) stabilizing fluid compositions and 5) small amounts of fluids being present in localized parts of the rock (Etheridge *et al.*, 1983; Schliestedt & Matthews, 1987; Bröcker, 1990; Barrientos & Selverstone, 1993; Parra *et al.*, 2002; Breeding *et al.*, 2003; Kleine *et al.*, 2014; Peillod, 2018). In the parts of the rock that have not been affected by re-equilibrating fluids, the mineral assemblage can be preserved metastably, even under P-T conditions in which they normally would not be seen.

The aim of this study was to analyse HP-LT (eclogite facies) rocks, outcropping on the coastline of Fabrika, Syros, Greece, where cross-cutting veins bearing alteration halos of lower metamorphic facies (blueschist and greenschist) are found. The focus of the study was to find out what caused these alteration haloes, seen at the selvages of the veins, to form and why they are of different metamorphic facies. The hypothesis formed was that there had been either two different vein forming events, at different P-T conditions, or fluids of two different compositions in the veins under similar P-T conditions, causing the difference in metamorphic facies seen in the haloes.

Regional Geology

The Hellenic Subduction System

The Hellenic subduction system is located in the eastern parts of the Mediterranean Sea. It formed during closure of the Tethys Ocean (along the Vardar suture zone), beginning in the Cretaceous (Matthews & Schliestedt, 1984; Robertson *et al*., 1991; Keiter *et al*., 2004; Jolivet & Brun, 2008; Vitale Brovarone *et al*., 2011) as a part of the Alpine orogeny, when convergence between Africa and Eurasia caused the African plate to subduct beneath the Eurasian southern margin.

The Hellenic subduction system can be sub-divided into five different zones (from north to south): 1) the Internal zone, 2) the Vardar-Izmir-Ankara suture zone, 3) the Pelagonian zone, 4) the Cycladic zone, and 5) the External Hellenides (Dürr *et al.*, 1978; Robertson *et al.*, 1991). The focus for this study is the island of Syros located in the Aegean Sea in the Cycladic zone (no. 4). For further information regarding the other zones, see e.g. Jolivet & Brun (2008) and references therein.

Aegean Sea and the Cyclades

The Aegean Sea formed as a back-arc basin in the mid-Cenozoic by lithospheric extension caused by the roll-back of the African slab that had been subducting beneath the Eurasian plate (Ring *et al*., 1999; Jolivet & Brun, 2008). This roll-back was a result of stalled convergence between Europe and Africa coupled with the continued subduction of the African plate due to slab pull (Jolivet & Brun, 2008). The combination of convergent and extensional forces in these parts of the Hellenic subduction system created the appropriate conditions needed for exhumation and preservation of rocks bearing a HP-LT mineral assemblage.

The region of the Cyclades, Greece is located in the Aegean Sea, and is therefore a part of the Hellenic subduction system (Ring *et al*., 1999; Jolivet & Brun, 2008; Kleine *et al*., 2014). Three tectonic units can be recognized in the Cyclades, which are, from top to bottom; 1) an ophiolitic nappe, that is only locally affected by low-grade metamorphism, 2) the Cycladic blueschist unit (CBU), composed of HP-LT subduction zone type rocks, and 3) the Basal Unit (Ring *et al*., 1999; Ring & Glodny, 2010).

The CBU represent the deepest now exhumed parts of the Hellenic subduction system (Ring *et al.*, 1999), except for the Kerketas nappe, cropping out only on the neighbouring island of Samos (Ring *et al.*, 1999). The CBU was exhumed to the lower crustal level as an extrusion wedge caused by thrust faulting (Ring *et al*., 1999; Ring & Layer, 2003; Jolivet & Brun, 2008; Ring & Glodny, 2010), i.e. exhumation of the CBU occurred under compressional tectonic forces, not in a regionally extensional setting. Shortly after the thrust faulting event the CBU was exhumed to the surface by low-angle normal faults (Ring *et al.*, 1999; Ring & Layer, 2003; Ring & Glodny, 2010). The exhumation of the CBU by thrust faulting, in association with overlying normal faults, is evident by the shear sense of the mylonitic fabric of the faults below and atop the CBU nappe (Ring & Glodny, 2010). The mylonites of both type faults have been dated to be of approximately the same age (~30 Ma, Ring & Glodny, 2010). The fact that the CBU is of higher metamorphic grade than the units found both above and below also support this being the sequence of events bringing the CBU to the surface.

The history of the Cyclades is a complex one with compressional and extensional forces, nappe stacking, asthenospheric upwelling causing thermal overprinting etc. For more information regarding the full development of the Aegean region see e.g. Ring *et al*. (1999) and Jolivet & Brun (2008).

Syros

The island of Syros, Greece is part of the Cyclades archipelago located in the Aegean Sea, south-west of mainland Greece (fig. 2a). Syros is mainly made up of well-preserved HP-LT rocks of blueschist and eclogite facies belonging to the CBU (fig. 2b) (Avigad *et* al. 1989; Keiter *et al.*, 2004; Jolivet & Brun, 2008; Philippon *et al*., 2011; Kleine *et al*., 2014; Cliff *et al.*, 2017; Peillod, 2018).

The CBU rocks in Syros consists of a top section of a meta-ophiolitic mélange, primarily derived from mafic to ultra-mafic protoliths, overlying a lower section of passive-margin sequence type rocks (Keiter *et al*., 2004; Philippon *et al*., 2011; Kleine *et al*., 2014; Peillod, 2018). The lower section is composed of a layered sequence containing rocks of both a volcanic as well as a sedimentary origin. The samples collected for this study belongs to this lower volcano-sedimentary section.

In Vari, located in the south-eastern parts of Syros, there is also a gneiss of Carboniferous age cropping out (fig. 2b) (Maluski *et al.*, 1987; Tomaschek *et al.*, 2003). It is unclear if this Vari gneiss is a remnant part of the Upper Cycladic unit (Avigad *et al.*, 1989; Jolivet & Brun, 2008), or if it should be considered a part of the Basal Unit (Philippon *et al.*, 2011).

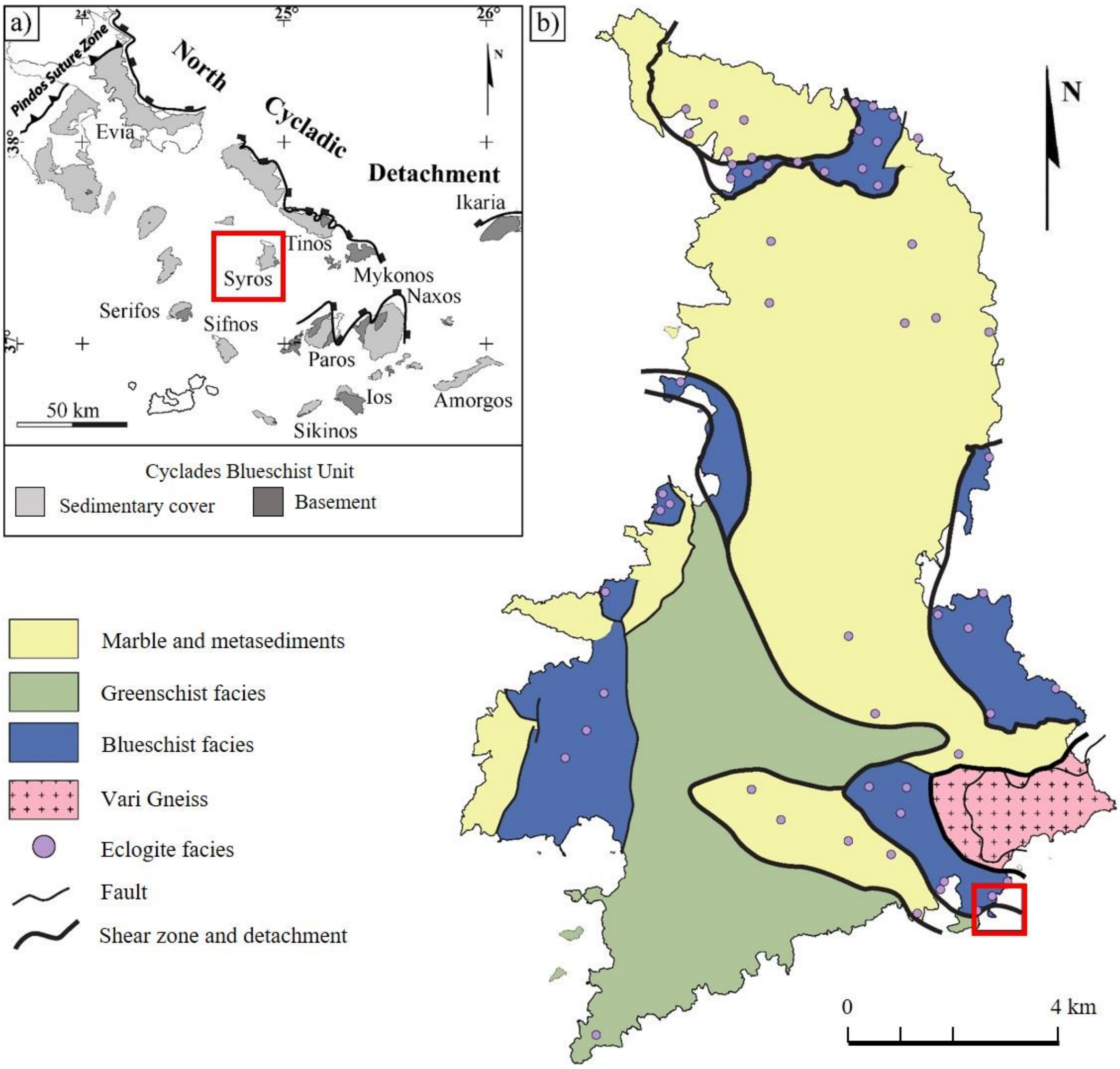

Fig. 2: a) Regional map of the Cyclades with Syros highlighted in red. b) Geological map of Syros with the location of Fabrika highlighted in red. Modified from Peillod (2018).

The blueschist and eclogite meta-basaltic rocks of Syros display a very similar P-T history (Behr *et al.*, 2018; Peillod, 2018), implying that the difference in facies seen in these rocks are due to compositional differences in the protoliths, rather than a difference in the P and/or T conditions experienced by the rocks.

At Fabrika, a prograde path going through lawsonite blueschist facies (at 1.1-1.4 GPa and 380-460°C) and into the epidote blueschist and eclogite facies (1.5-1.8 GPa and 470-500°C) has been described by Peillod (2018, fig. 3), where peak P-T of the now outcropping CBU rocks was reached. This peak P-T estimate correspond to that of Schumacher *et al*. (2008), who calculated peak P-T conditions of 1.5-1.6 GPa and 500°C, but differs from the 2.2 ± 0.2 GPa and 530 ± 30°C calculated by Laurent *et al.* (2018). The peak P metamorphism of the CBU found in Syros has been dated as occurring in the Eocene (53-52 Ma Tomaschek *et al*., 2003, ~50 Ma Jolivet & Brun, 2008, and 43-38 Ma Peillod, 2018).

Retrogression occurred at greenschist facies conditions (0.34 ± 0.21 GPa and 456 ± 68°C, Peillod, 2018, fig. 3) and is associated with hydration and metasomatism of the rocks. This event has been dated as occurring at early Miocene to mid Oligocene times (~20 Ma Altherr *et al.*, 1979, ~27 Ma Peillod, 2018).

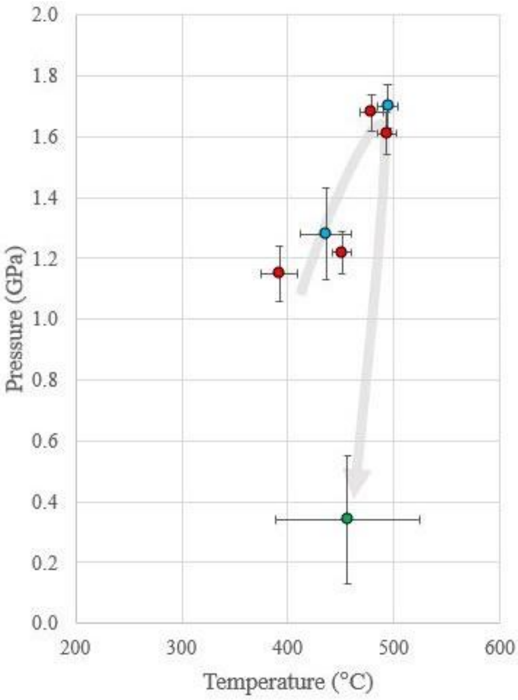

Fig. 3: Estimated P-T loop from Peillod (2018).
Red: eclogite samples, blue: blueschist, green: greenschist

The greenschist facies retrogression was only partial and did not affect the entire rock volume since HP-LT rocks in Syros are still preserved. The reason for this could be, as mentioned above, lack of metamorphic fluids, impermeable rock layers and/or highly channelized fluids along conduits, as well as metamorphic fluids of a composition that aids stabilization of the HP-LT minerals outside their stability field, had the fluids been comprised of H_2O alone. In Syros several of these preserving factors can be found, e.g. impermeable marble layers, fluids channelized via conduits (there is e.g. ultramafic knockers located at one outcrop by the Fabrika coastline, indicating the presence of a large shear zone cutting through Fabrika beach where the rocks outcropping have been completely reset to greenschist facies), and fluids of a composition stabilizing blueschist facies mineral assemblages, as was found by Kleine *et al*. (2014) close to the greenschist facies bearing shear zone aforementioned.

The P-T-t of the metamorphic events on Syros are similar to those described from islands nearby (e.g. Sifnos by Matthews & Schliestedt, 1984, and Naxos by Peillod *et al.* 2017)

Fabrika

The outcrop studied for this thesis is located at Fabrika beach in the south-eastern part of Syros. The rocks here, as most rocks on Syros, belong to the CBU and are primarily of eclogite and blueschist facies (fig. 4), often interlayered on a cm-m scale. This layering could represent a relict passive margin volcano-sedimentary bedding with alternating variably mafic volcanogenic or carbonate-clastic sediments as protoliths (Schumacher *et al.*, 2008; Kleine *et al*., 2014; Peillod, 2018).

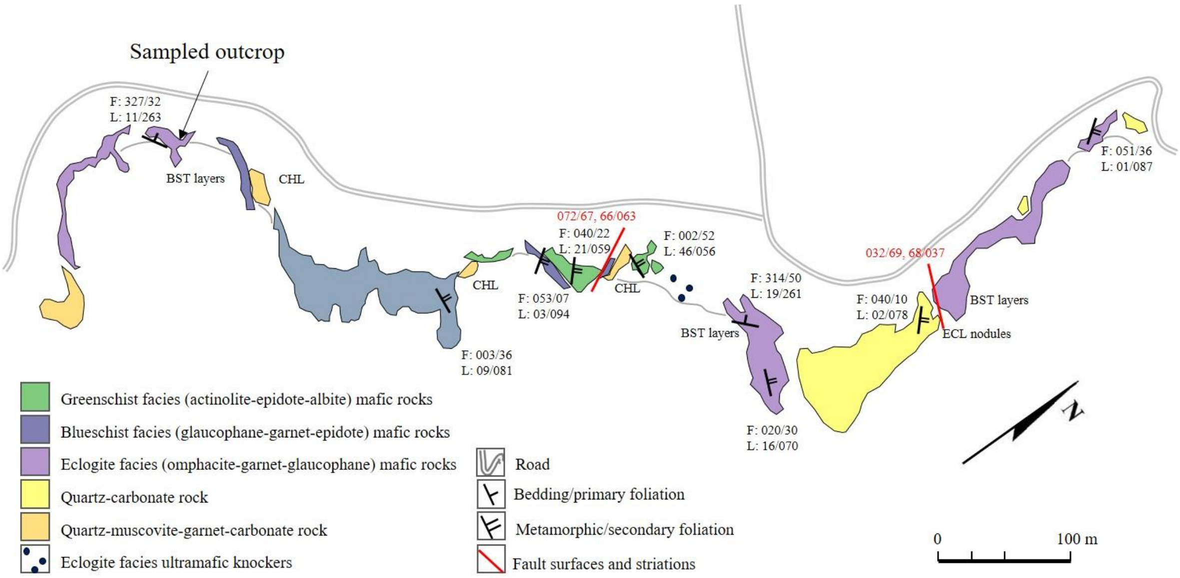

Fig. 4: Geologic map of the coastal section, Fabrika beach, SE Syros. Foliations (F): Three digit no. for dip direction, two digit no. for dip angle. Lineation (L): Two digit no. for plunge, three digit no. for trend. BST: blueschist, ECL: eclogite, CHL: chlorite. Modified from Peillod (2018).

Studied outcrop

The outcrop studied for this thesis is located at N 37° 23.290´, E 24° 57.109´ at Fabrika, Syros.

The outcrop from where the samples were collected is a metamorphosed layered sequence of mafic volcanogenic-, and carbonate rich sedimentary rocks. The layers with a mafic protolith are seen as (primarily) eclogites and (minor) blueschists, while the carbonate rich layers are composed of quartz and carbonate minerals (fig. 5 and 6). Several reaction halo bearing veins cross-cut the outcrop in what seems to be two distinct directions (fig. 6). These reaction halos were interpreted as being of greenschist and blueschist facies based on their colour and mineralogy in the field.

Cross-cutting relationships were sought after in the field, in order to determine the relative age of the veins sampled, and, by doing so, be able to tell which of the vein orientations, and associated halo facies, were the older/younger. The interpretation made was that some veins bearing a greenschist halo (oriented top right-bottom left in fig. 5 and 6) were cross-cutting the veins with blueschist halos (oriented vertically in fig. 5 and top left-bottom right in fig. 6), and therefore the greenschist-bearing veins were the younger of the two, but there was no way, in the field, of determining the time span between the formation of these veins. In addition to this, some of the greenschist-bearing veins were striking in the same direction as the blueschist-bearing veins, and were also cut by other greenschist-bearing veins (fig. 5). Due to this, the field conclusion was that the veins striking vertically were older, but any halo-facies associated age relationship remained unclear.

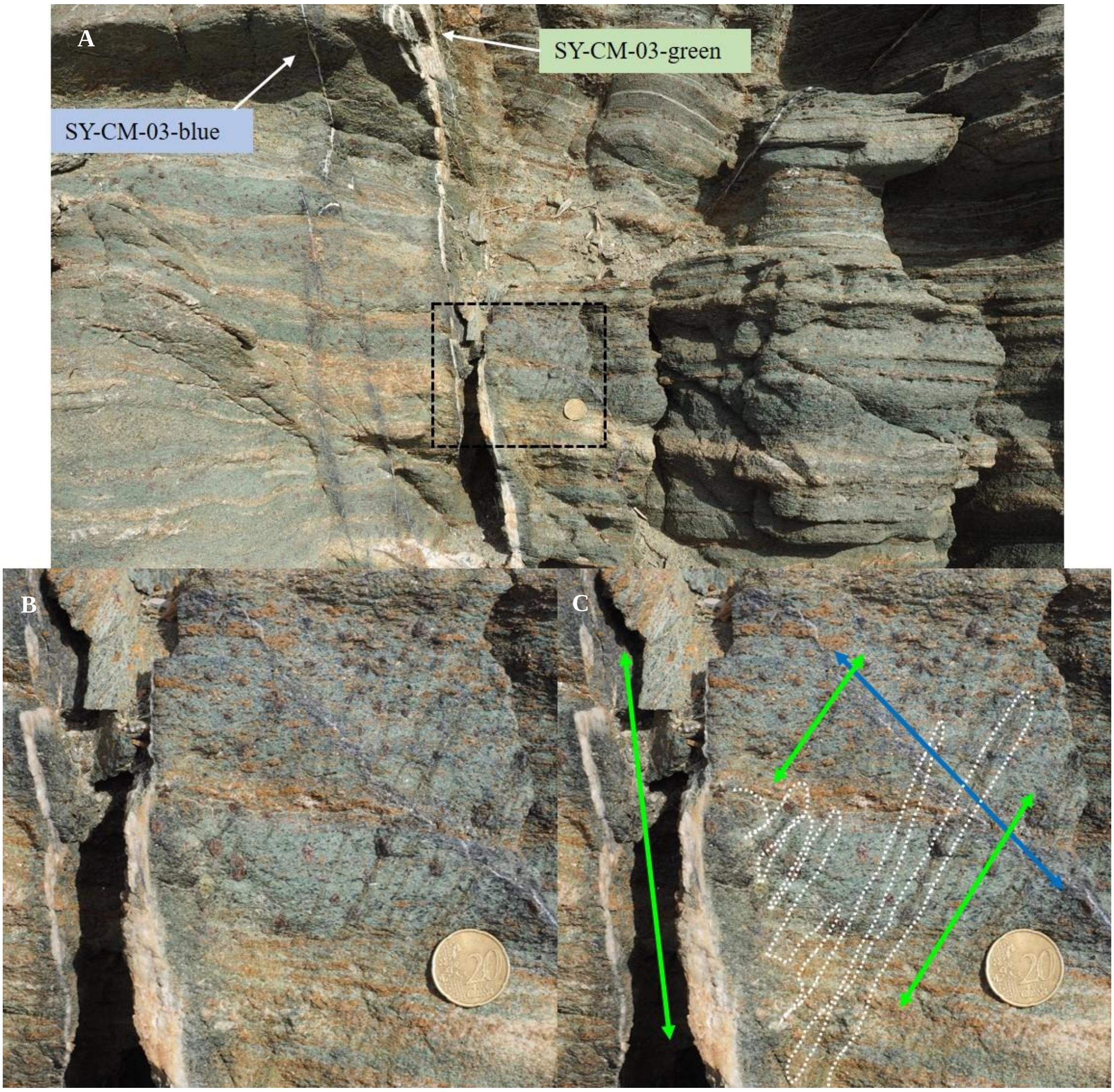

Fig. 5: Small veins with greenschist haloes (outlined in C) emanating from a larger greenschist-bearing vein and cross-cutting a vein with a blueschist halo, as indicated by different coloured arrows in C. B and C are close-ups of area indicated by square frame in A. €20 cent coin for scale. Photos by Alasdair Skelton.

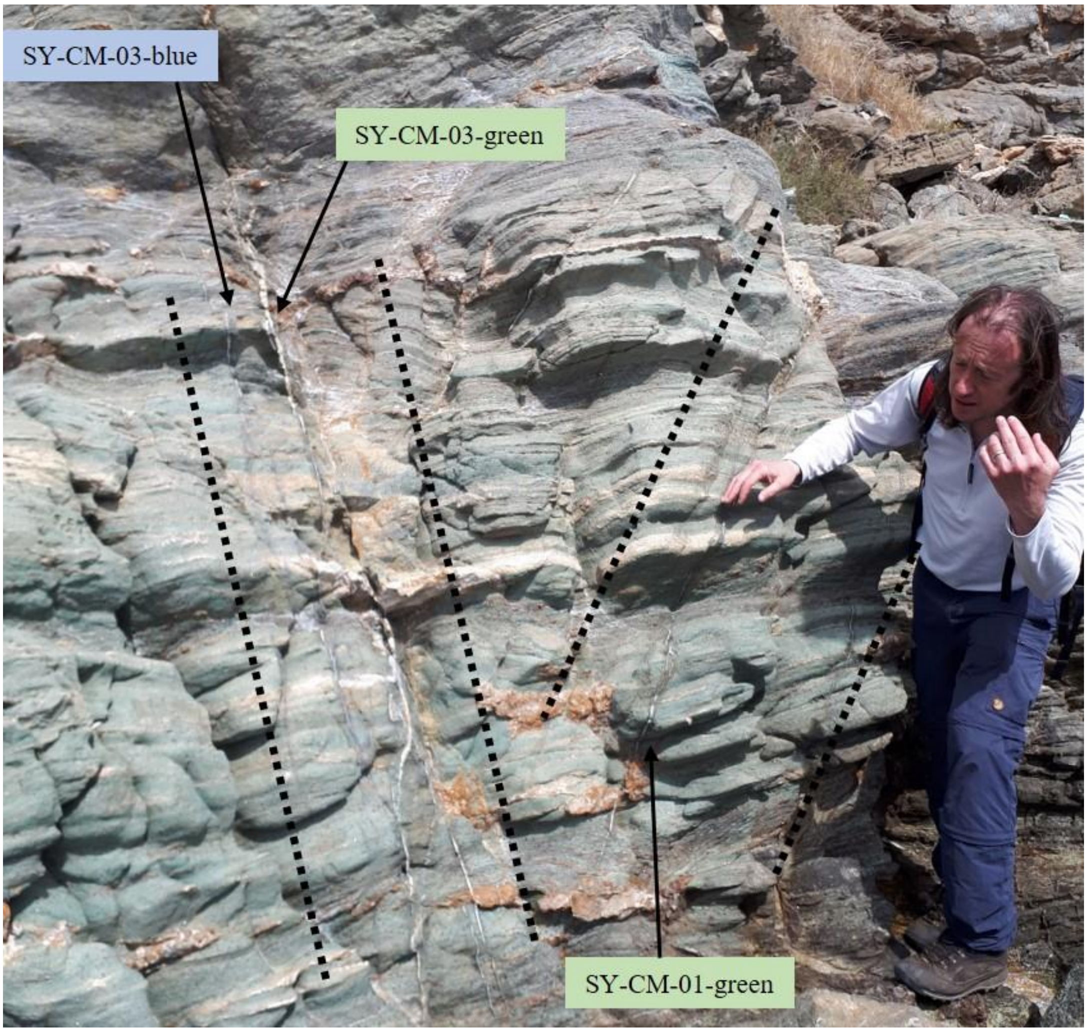

Fig. 6: Location of samples in the outcrop with the two different strikes of sampled veins indicated by dotted lines. The veins oriented top left-bottom right in the photo represent the orientation of the SY-CM-03 samples, the top right-bottom left oriented veins represents the orientation of sample SY-CM-01. Colour of background of sample name indicates blue or green halo.

Methods

<u>Sampling</u>

The outcrop in focus was visually inspected in order to identify the best samples to collect for the purpose of this study. Three different veins with reaction halos were selected for sampling. Two of the samples were in the field interpreted as bearing greenschist halos and one was interpreted as having a blueschist halo. These interpretations were done from visual inspection of the colour of the halo as well as identification of the mineralogy of the halos using a 10x magnifying hand lens.

The rock samples were then carefully collected using a hammer and chisel in order not to crack the rocks along the veins, which could have resulted in a loss of parts of the reaction halos surrounding the veins. The samples collected were then individually placed in zip-lock bags that had been marked with a sample ID.

Cutting of samples/Thin sections

The collected rock samples were transported to Stockholm University. From each sample at least two thin sections of vein haloes were made. These were all labelled with an individual sample ID (e.g. SY-CM-01-01-green, SY-CM-01-02-green etc.) and shipped to Vancouver Petrographics, Canada for the thin sections to be produced.

Analysis

Scanning of samples
The rock samples were scanned along the cut surface using an Epson Perfection 2400 Photo scanner and the Epson Smart Panel software in order to get a complete image of the samples.

Scanning of thin sections
The thin sections were scanned using a Nikon Super Coolscan 9000 ED scanner and the Nikon Scan 4.0.2 software. The clarity of these images was enhanced using the Adobe Photoshop CC software.

Point counting
To estimate the modal abundance of the minerals in the host rock, reaction halos and veins, point counting of the thin sections were done using a Leica light microscope, with a Pelcon automated stage set to an interval of 0.5 mm, and the PelconPointCounter 9 version 2.00 software. In the host rock samples, 500 point were counted, in the haloes 300 or 500 counts were made and in the veins 100 or 200 points were counted (see tables 5A, B, and C in appendix). Errors were estimated using the method of van der Plas & Tobi (1965) (tables 5A, B, and C in appendix).

Photo-microscopy
Photomicrographs of the thin sections were taken using the Leica Nikon Optiphot2-POL Polarizing Transmitted Light Microscope and the Leica Application Suite LAS EZ version 3.4.0 software.

Visual analysis/microscopy
Visual analysis of the thin sections was done using the same Leica Nikon Optiphot2-POL Polarizing Transmitted Light Microscope that was used for taking photomicrographs.

Results

Mineral abbreviations are from Whitney & Evans (2010, see appendix for abbreviations used). All modal abundance figures are from point counting of the thin sections.

In sample SY-CM-03 there were two veins present, one with a blueschist halo (SY-CM-03-blue) and one with a greenschist halo (SY-CM-03-green). These samples were situated just cm´s apart (fig. 5A and 6). Sample SY-CM-01-green was collected from the same outcrop, ~1m from the other samples (fig. 6), and the vein in this sample had a greenschist halo.

SY-CM-01-green

Host rock

The matrix of the host rock is very fine grained and has a minty green colour, as well as a silky shine. The green colour is from Cpx (Omp), while the silky shine is due to fine grained Wm, both of which makes up for a large part of the modal abundance of the matrix (table 1). The host rock of the sample is, due to the high modal abundance of Omp, and the presence of Grt, interpreted as being an eclogite facies meta-basalt (Eskola, 1920).

Within the fine grained matrix some porphyroblastic minerals can be seen:

- Grt:
  2-9 mm wide, euhedral, ~equidimensional, patchily distributed throughout the sample.
- Gln:
  Lath shaped, 1-5 mm in length and 0.5-1 mm in width, displays a preferred orientation parallel to the foliation of the rock.
- Wm:
  0.5-3 mm in length and 0.25-3 mm in width, no preferred orientation.

The host rock has a weak metamorphic foliation, which is inclined with respect to the vein of the sample (fig. 7). Orange alteration streaks can be seen throughout the sample, which run along foliation planes (fig. 7 and 8). These alteration streaks are due to a later stage alteration of Cal into Dol (Schumacher *et al.*, 2008).

This alteration is also seen along later formed cracks, cross-cutting the vein (fig. 7A). The cracks are oriented in a fashion that could imply that they formed as a conjugate set of fractures (Bons *et al.*, 2012). If so, the orientation of the cracks could be used to find $\sigma 1$, $\sigma 2$, and $\sigma 3$ for the deformation event that caused them. The fact that these are brittle, and not ductile, features reveals that the deformation causing the cracks occurred while the eclogite host rock was at P-T conditions causing a brittle behaviour of the minerals, while the cross-cutting of the main vein reveals that they formed at a later stage than the vein.

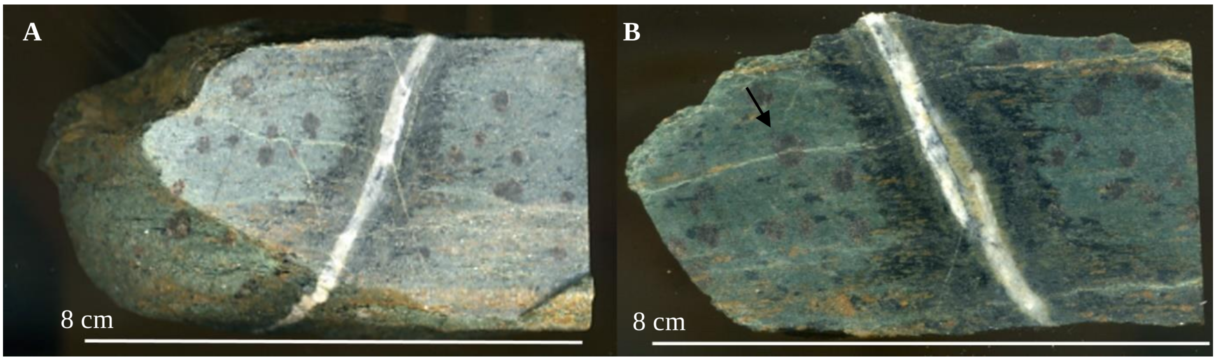

Fig. 7: A: Conjugate (?) fracture sets. B: Small fluid filled crack along a foliation plane splitting a Grt porphyroblast (indicated by arrow). The orange alteration, from dolomitization of Cal, is best seen at the bottom right of A, and top right corner of B.

Infiltration of fluids into the host rock have resulted in small "veins" forming along foliation planes (fig. 7B), which have caused a widening of the rock. This widening of the rock split up some porphyroblasts (e.g. the split Grt by the arrow in fig. 7B), indicating that this infiltration/deformation took place after the growth of the Grt porphyroblasts and under P-T conditions where the host rock minerals were acting in a brittle fashion.

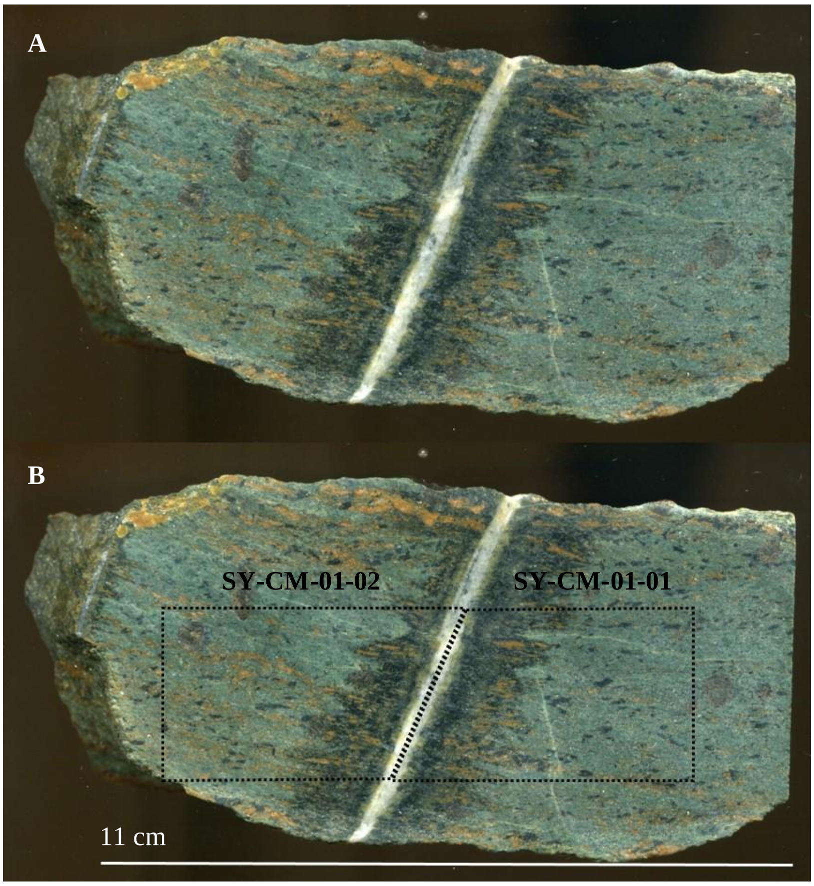

Fig. 8: A) Photo scanned cross-section of the SY-CM-01-green sample.
B) Outlines showing the approximate position of thin sections SY-CM-01-01/-02

The point counting shows that the most abundant minerals in the host rock are Omp, Ep, Wm and Grt (43.8% (3.14), 20.1% (2.53), 14.2% (2.21), and 8.4% (1.75) (error) respectively, summarized values, table 1. Individual thin section values presented in table 5A in appendix). Small amounts of Qz, Cal, Gln, Chl and Spn are also seen in the host rock samples.

Alteration into Cal can be seen in many minerals in the host rock, indicating that the reactions present record infiltration of a hydrous CO_2-bearing fluid. Qz is often found in association with Cal.

Omp is only found as small, matrix-sized crystals, but is of high modal abundance (table 1). Alignment of Omp crystals defines the aforementioned metamorphic foliation. This indicates that the Omp is pre- or syn-tectonic. Omp can also be seen as inclusions in porphyroblasts, e.g. in the Amp crystal in fig. 9.

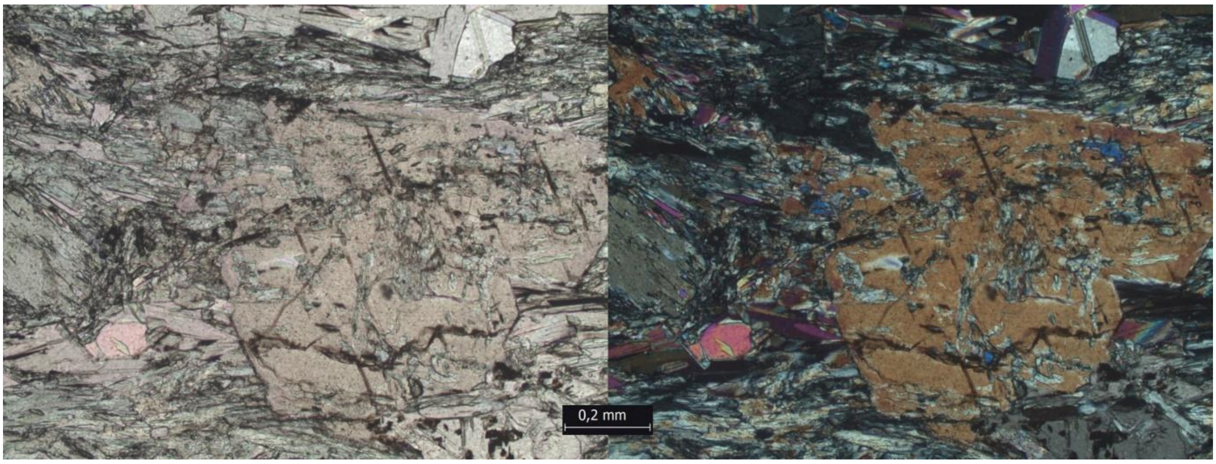

Fig. 9: Inclusions of Omp in an Amp porphyroblast in sample SY-CM-01-01. PPL to the left, XPL to the right.

Wm is present both as porphyroblasts and as smaller, matrix-sized crystals. The preferred orientation of the matrix-sized Wm is the same as that of the Omp, i.e. parallel to the metamorphic foliation. The porphyroblastic Wm are randomly orientated. The different sized Wm are interpreted as being of different generations and compositions. This interpretation is based on the difference in size and orientation, as well as the porphyroblastic Wm displaying disequilibrium features, being altered into Cal and Qz, ± Cal (fig. 10). Some of the porphyroblastic Wm have inclusions of Omp.

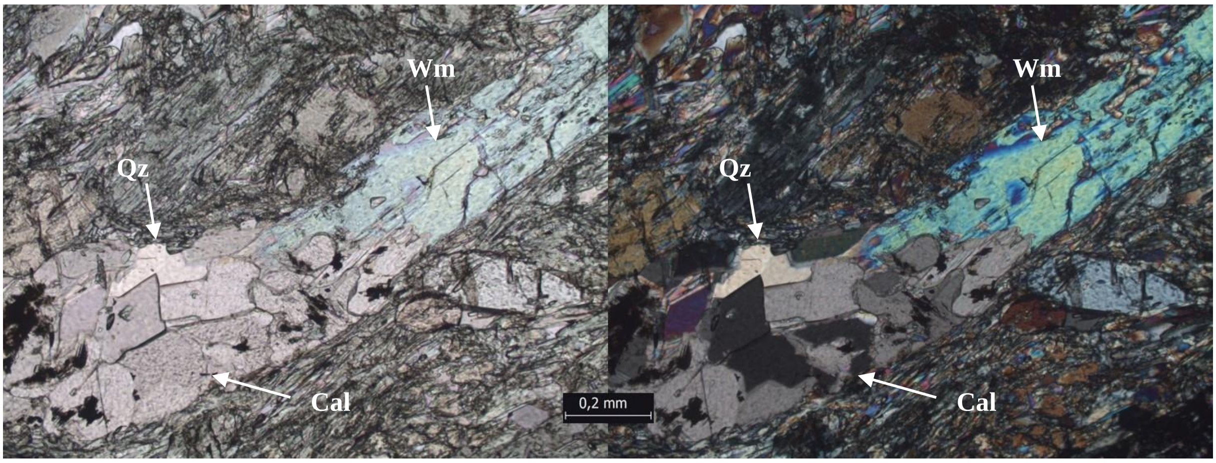

Fig. 10: Wm porphyroblast altering into Cal and Qz in eclogitic host rock of sample SY-CM-01-02. PPL to the left, XPL to the right.

The Ep porphyroblasts are euhedral-subhedral in the host rock, and have inclusions of Omp, i.e. they are poikiloblasts. The Ep poikiloblasts might be of two different generations since they seem to have two different preferred orientations, where one is aligned parallel to the foliation and the other is at an angle to it (fig. 11).

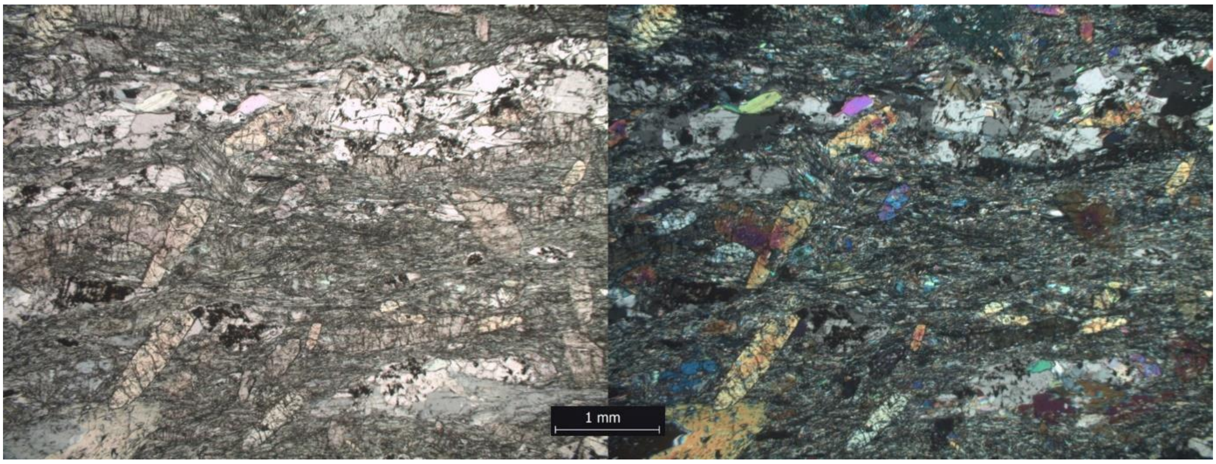

Fig. 11: Overview of the eclogite host rock from sample SY-CM-01-01, showing the metamorphic foliation as well as Ep porphyroblasts of different preferred orientations. PPL to the left, XPL to the right.

Ep is seen as altering into Qz and Cal, ± Chl (fig. 12). The Ep crystals are euhedral-subhedral in shape, which indicates that the re-equilibration of Ep in the host rock is only minor.

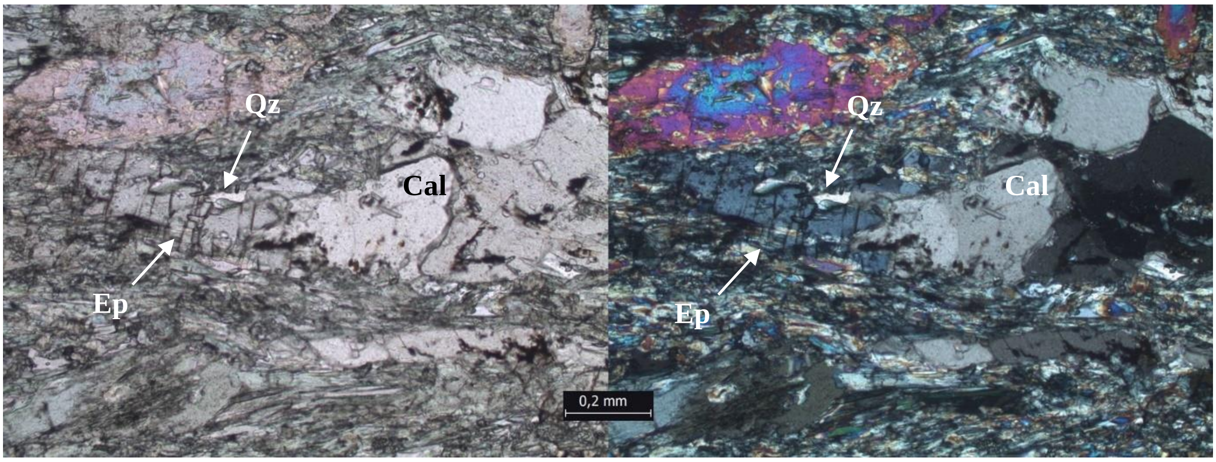

Fig. 12: Ep into Cal and Qz in host rock of sample SY-CM-01-01. PPL to the left, XPL to the right.

The porphyroblastic Grt are euhedral-subhedral and have inclusions of Omp, Gln, Ep, Spn and Zrn, i.e. they are poikiloblasts. The inclusions are mainly in the centre of the crystals, with a rim displaying a lesser abundance of inclusions (fig. 13). This difference in the abundance of inclusions implies that a change in the Grt forming reaction has occurred, from the centre to the rim, where the mineral types present as inclusions at the centre, at a later stage instead have been consumed to form the rim of the Grt. The inclusions of Omp, Gln, and Ep put the nucleation and initiated growth of the Grt poikiloblasts at HP-LT conditions. In places, pressure shadows can be seen next to the Grt. This indicates that at least one deformation event took place after the growth of the Grt poikiloblasts, with dissolution-precipitation of surrounding minerals. Grt, Wm and Ep are intergrown (fig. 13C and D), and are, in places, being altered into Cal and Chl.

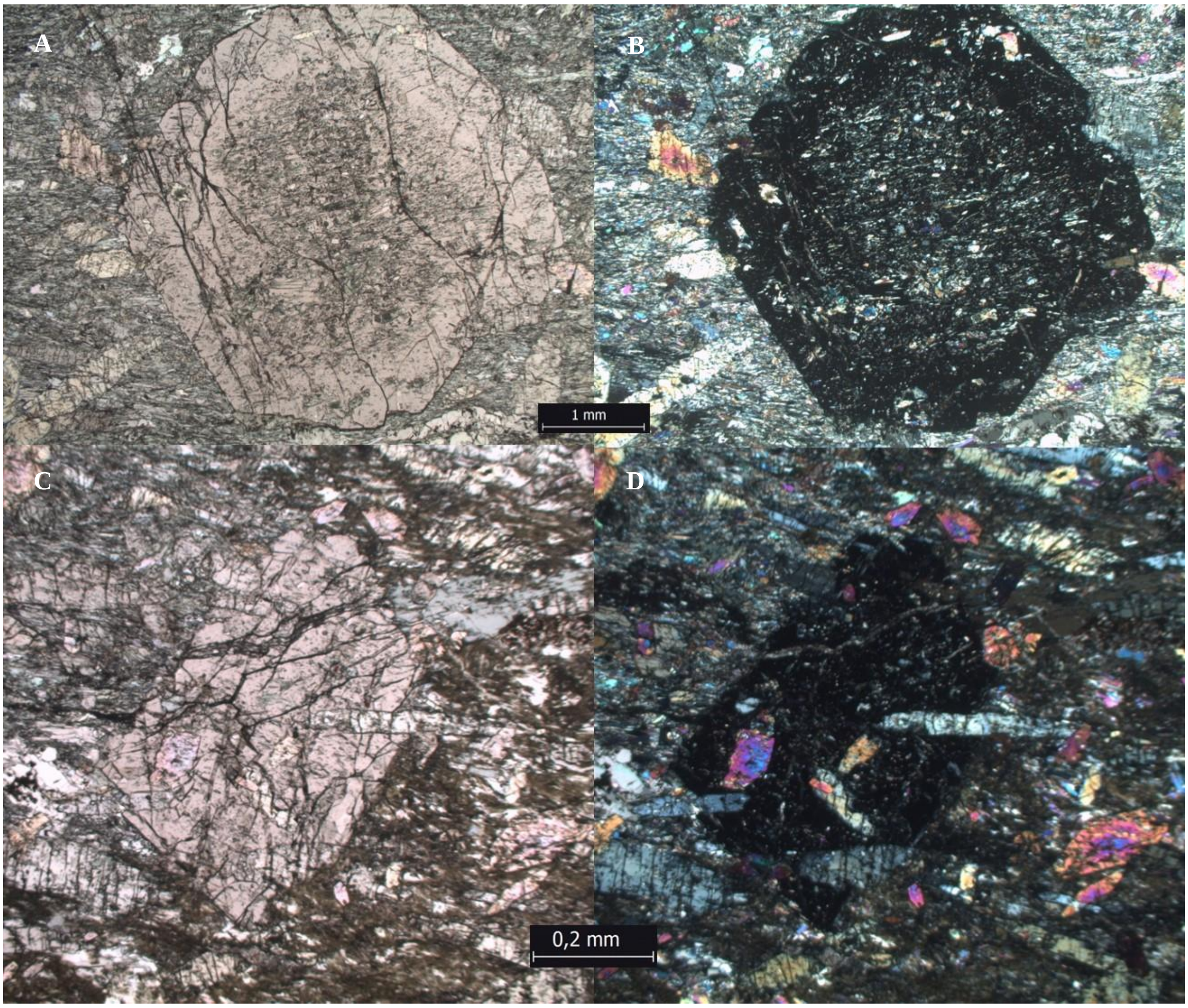

Fig. 13: A and B) Poikiloblastic Grt in host rock of sample SY-CM-01-01 with an inclusion rich centre, and a rim displaying a lower abundance of inclusions. C and D) Intergrown porphyroblasts. PPL to the left, XPL to the right. Note the difference in scale.

Small amounts of Gln are present, but only close to Grt, and typically adjacent to the halo. The reason that Gln only can be seen close to Grt is most likely due to the large Grt crystals protecting the Gln from alteration. Inclusions of Omp can be seen in some of the Gln.

In parts of the host rock small veins can be seen cross-cutting the eclogite, causing chloritization of the surrounding minerals (fig. 14). Since these veins cut all other minerals, as well as the foliation, they are interpreted as being a product of a later stage deformation event than the one that caused the foliation to form, perhaps the same event that resulted in the formation of the larger vein seen in the sample. This reasoning can be supported by the sub-vertical small vein in fig. 14, and the larger vein striking in the same direction.

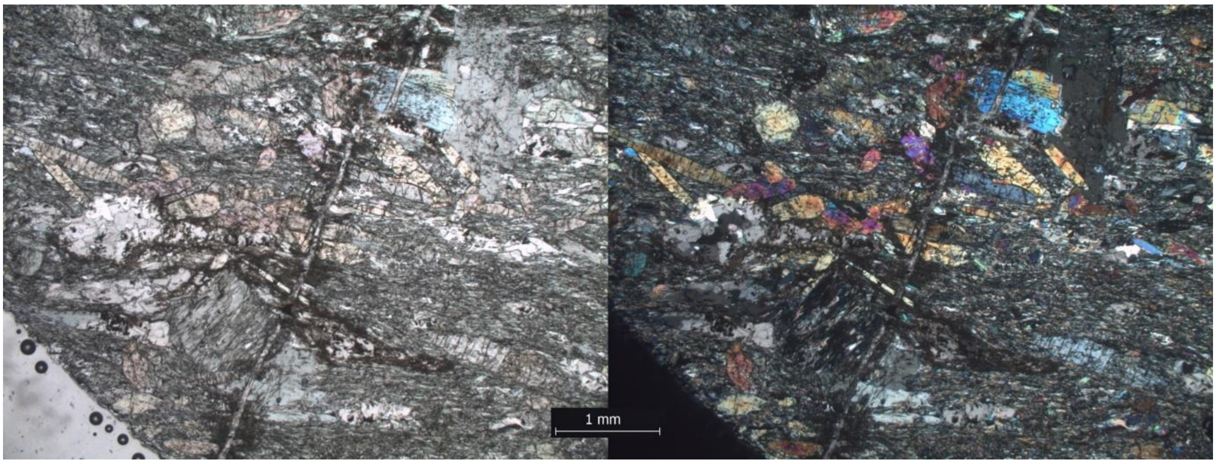

Fig. 14: Cross-cutting vein in host rock causing hydration and chloritization of surrounding minerals. From sample SY-CM-01-02. PPL to the left, XPL to the right

Qz, Ep, and Cal display undulose extinction. This in combination with grain boundary migration (GBM) and recrystallization in Qz, the matrix minerals being deflected around the porphyroblasts, as well as the matrix minerals defining the foliation, indicates that the bulk of minerals in the host rock are pre- to syn-tectonic, i.e. the bulk of minerals most likely predates, or are synchronous to, the foliation forming deformation event. Most of these deformation features can also be seen in the halo.

Vein

The boundaries between the halo and the vein are well defined and no deflection of the foliation on either side of the vein is seen. The vein has a constant width of ~3 mm throughout the sample, except for in a few places where the vein has been deformed. In the deformed places, the measured width is up to 4 mm (middle of vein in fig. 7B). The lack of deflection of the halo minerals into the vein, along with the constant width of the vein, suggests that this vein formed from a deformation event that took place under P-T conditions where the host rock and halo behaved in a brittle fashion.

The resistance to weathering processes seems to be higher in the vein in comparison to the host rock and halo, where it seems to be approximately the same. This can be seen by the vein protruding out of the rock on the weathered surfaces.

The point counting shows that the vein is comprised primarily of Cal and Qz (table 1). Since the vein contains both Qz and Cal, the fluid must have been hydrous and carbon bearing, including CO_2 as a constituent.

The Opq of this vein are primarily found along the edges of the vein (fig. 15).

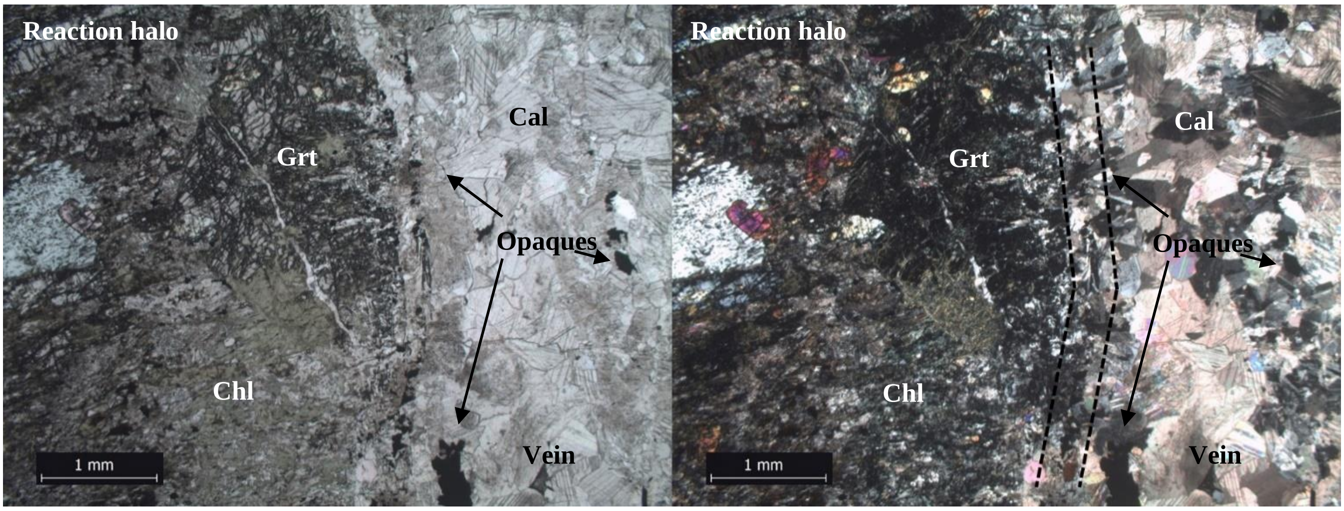

Fig. 15: Opaques crystallized by the edge of the vein (and some in the vein), to the right indicated by dotted lines. A highly altered Grt can be seen in the vein/halo transition. PPL to the left, XPL to the right.

Small amounts of Pl, Wm, Ep, Chl and Omp are also present in this vein (table 1). Pl is believed to be albite (Schumacher *et al.*, 2008; Kleine *et al*., 2014), and is interpreted as being a product of a reaction between the vein fluid and the host rock, since it is not present in the host rock or halo (table 1) and is lining the vein. Wm, Ep, Chl and Omp are all interpreted as being remnant host rock minerals, and in disequilibrium since these minerals display very low modal abundances, as well as highly altered, anhedral forms.

Cal crystals display a range in size. Pl and Cal are intergrown (fig. 16). The Qz present is primarily found in association with Pl and Cal. Pl, Cal, and Qz have a speckled appearance (fig. 16), indicating that they are in disequilibrium.

Both Cal and Qz display some deformation features (e.g. undulose extinction and GBM) caused by strain in the crystal lattices from (a) deformation event(s). This suggests that the rocks have been subjected to deformation after the crystallization of the vein forming minerals.

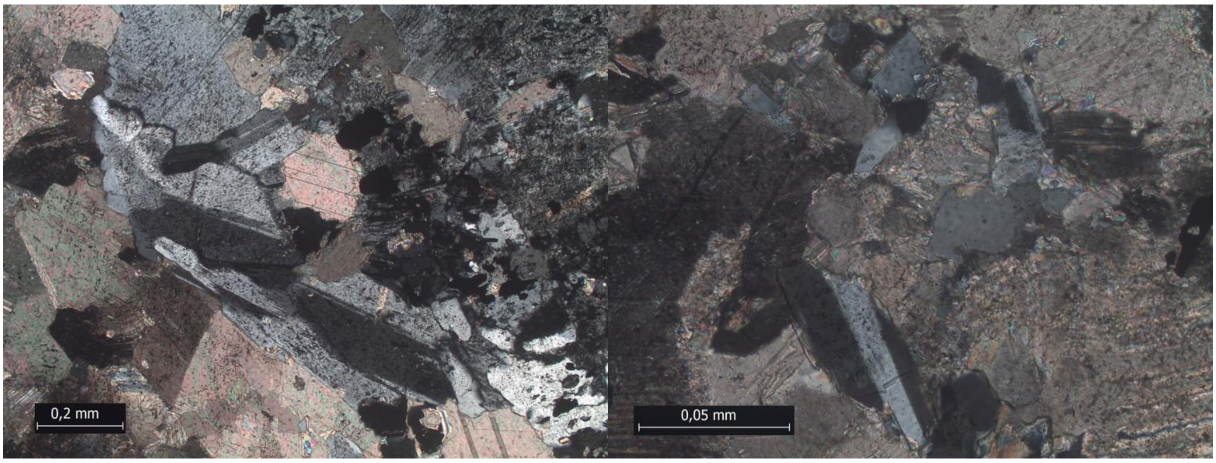

Fig. 16: Intergrowth of Pl, Cal and Qz in sample SY-CM-01-01.Both fig. in XPL. Note the difference in scale in the two figures.

Reaction halo

This halo contains greenschist facies minerals (Eskola, 1920). Fine grained Chl is abundant (table 1), giving the rock a deep green colour that is distinct from the green colour of the eclogite host rock (fig. 7 and 8). The halo also contains Ep (table 1).

The width of each halo ranges from 0.5-20 mm. The widths of the halos on either side of the vein are similar (fig. 7 and 8), suggesting that the fluid infiltration from the vein and into the host rock was approximately the same on both sides.

The halo displays some small differences in colour, where the greenest parts are seen closer to the vein, and the outer parts of the halo displays the later stage dolomitization described in the host rock (Schumacher *et al.*, 2008), giving parts of it a rusty orange colour (fig. 7 and 8).

The trend of the foliation is the same as in the host rock (cross-cut by the vein). Some surviving porphyroblasts of Grt, Wm, and Gln can be seen within the halo.

The minerals with highest modal abundances from the point counting are Chl, Cal, Ep and Wm (44.6% (3.51), 18.4% (2.74), 15.8% (2.58), and 7.8% (1.89) (error) respectively, summarized values, table 1) which supports the greenschist classification (Eskola, 1920) made in the field. However, the halo also contains smaller amounts of Omp, Qz, Grt, Gln, Spn, and Opq.

Comparison between the summarized modes of the halo and host rock (table 1 and 4) show decreases in Omp (-39.8%), Wm (-6.5%), Ep (-4.3%) and Grt (-4.5%) modes and increases in Chl (+43.9%) and Cal (+13.3%) modes.

This implies that Omp, Wm, Ep and Grt are replaced by Chl and Cal in the halo. This is supported by the following textures:

1. Omp is almost completely altered into Chl, Cal and Qz (fig. 17C and D) in the halo.
2. Porphyroblastic and matrix Wm are partly replaced by Chl and Cal (fig. 18A and B).
3. Poikiloblastic Ep is partly replaced by Chl ± Cal (fig. 18C and D).
4. Grt is partly replaced by Chl ± Cal (fig. 17A and B)

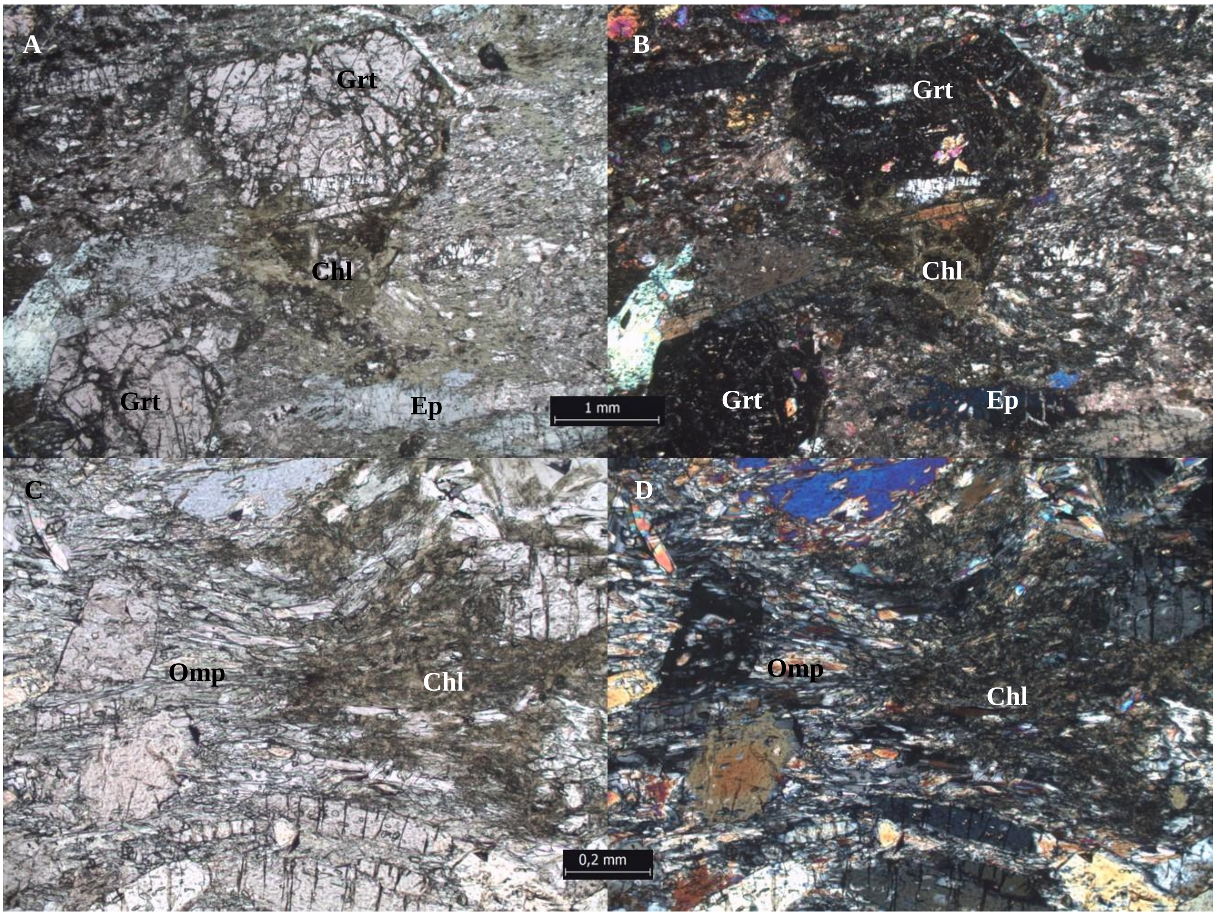

Fig. 17: A and B) Grt altering into Chl. A pressure shadow of precipitating minerals can be seen to the left of the Grt porphyroblast and the relict shape of the Grt can still be seen. The intergrown relationship between the porphyroblastic minerals can also be seen. C and D) Omp altering to Chl in the host rock-halo transition. Left side in PPL, right side in XPL. Note the difference in scale.

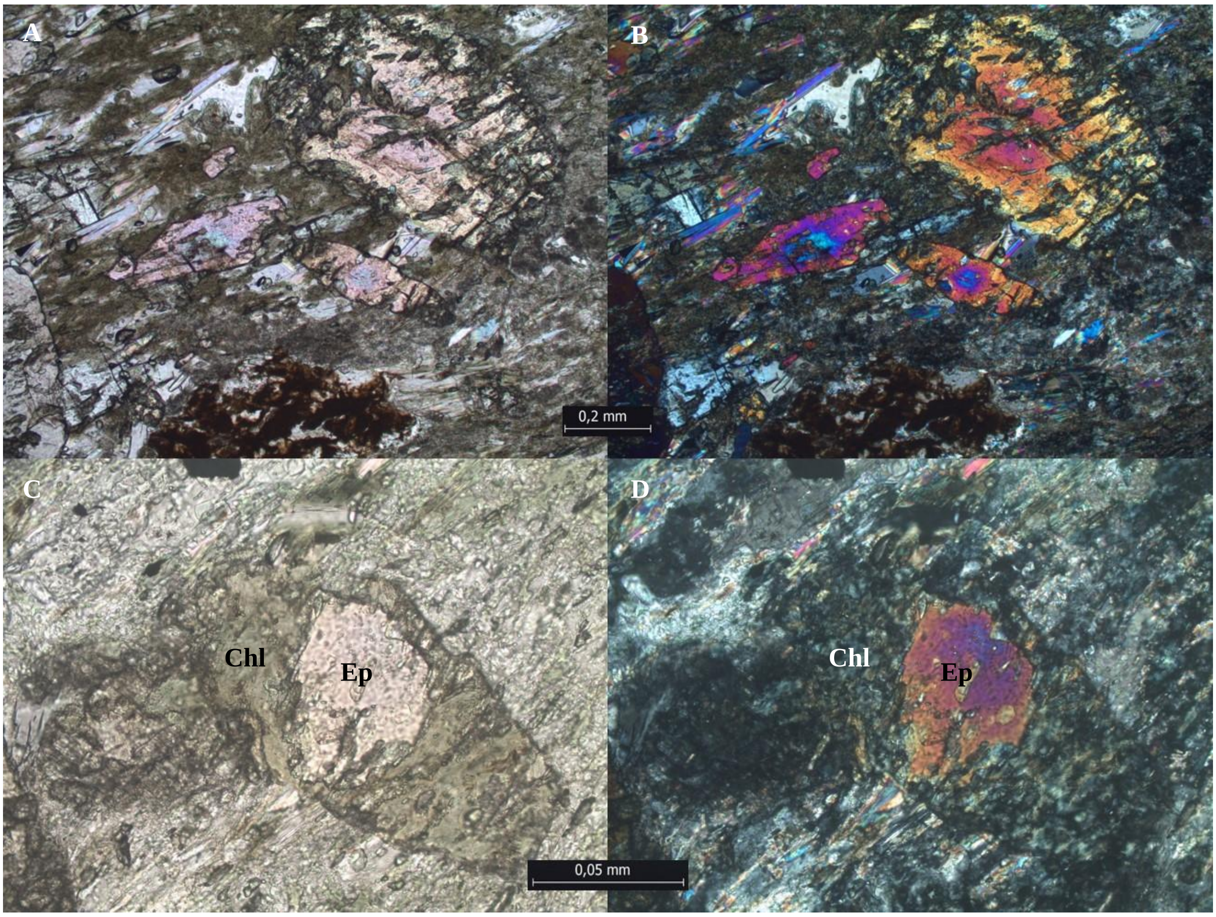

Fig. 18: A and B) Ep and Wm altering into Chl and Cal. C and D) Porphyroblastic Ep being altered/hydrated into Chl. Left side in PPL, right side in XPL. Note the difference in scale.

Overview of the thin sections of the sample provided in fig. 19.

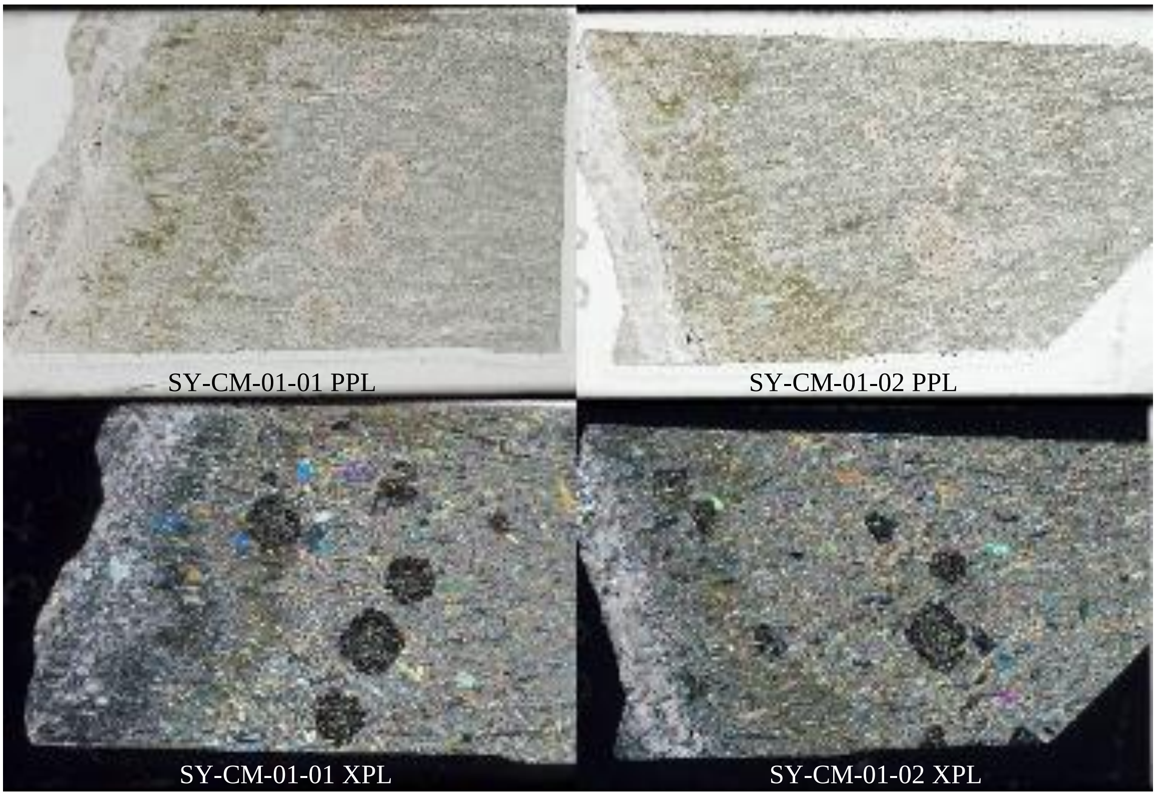

Fig. 19: Scanned images of thin section samples SY-CM-01-01/-02.

Table 1: Modal abundance result from point counting of thin sections SY-CM-01-01 and SY-CM-01-02. Numbers in percent. For individual thin section counts see table 5A in appendix.

SY-CM-01-green

	Host total	error	**Halo total**	error	**Vein total**	error
Epidote	20.1	2.53	15.8	2.58	0.3	0.50
Omphacite	43.8	3.14	4.0	1.39	0.8	0.86
Glaucophane	0.8	0.56	0.6	0.55	-	-
Carbonates	5.1	1.39	18.4	2.74	61.0	4.88
Quartz	3.3	1.13	1.8	0.93	23.0	4.21
Garnet	8.4	1.75	3.9	1.36	-	-
White mica	14.2	2.21	7.8	1.89	1.0	0.10
Sphene	3.6	1.18	1.9	0.97	-	-
Chlorite	0.7	0.53	44.6	3.51	1.3	1.11
Opaque	-	-	1.4	0.83	4.0	1.96
Plagioclase	-	-	-	-	8.8	2.83
	1000p 100%		800p 100%		400p 100%	

SY-CM-03-blue

Host rock

The host rock of this sample was interpreted as being an eclogite facies meta-basalt. This interpretation was done due to the modal abundance of fine grained Omp, giving the matrix a minty green colour, and the presence of Grt (Eskola, 1920). The sample also have a shimmer from fine grained Wm.

The porphyroblasts seen in this sample are:

- Grt:
  2-6 mm wide, euhedral, ~equidimensional crystals, patchily distributed throughout the sample.
- Wm:
  1-5 mm in length, 0.5-2 mm in width, and lath shaped, randomly oriented relative to the foliation, i.e. no preferred orientation can be inferred.

Orange alteration streaks can be seen throughout the sample, which run along foliation planes (fig. 20). This is due to the aforementioned late stage alteration of Cal into Dol (Schumacher *et al.*, 2008)

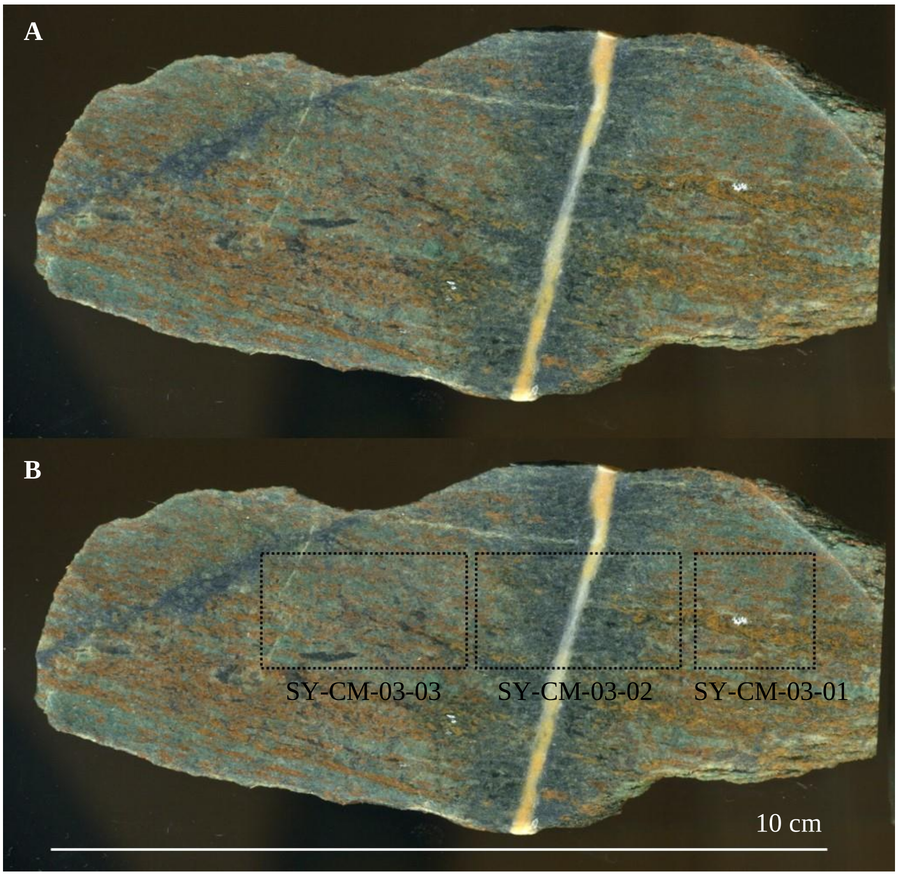

Fig. 20: A) Photo scanned cross-section of the SY-CM-03-blue sample.
B) Outlines showing the approximate position of thin sections SY-CM-03-01/-02/-03

Patches comprised of Cal and Qz, as well as some of monomineralic Qz, are present in in this sample, e.g. fig. 21.

Fig. 21: Monomineralic patches of Qz on the weathered surface of sample SY-CM-03-blue.

Point counting and visual analysis of the thin sections confirms the classification made in the field, i.e. the host rock is of eclogite facies.

The most abundant minerals are Ep, Cal and Omp (29% (2.87), 27.5% (2.82) and 19.6% (2.51) (error) respectively, summarized values from point counting of two thin sections, table 2). Qz and Wm are less abundant (10.6% (1.95) and 8.2% (1.74) (error) respectively, summarized values from point counting, table 2), and Grt, Spn, Chl and Gln only occurring as minor phases (table 2 and 4).

The host rock is affected by fluid infiltration, causing a lot of reactions to occur, and these samples are therefore not representable for a "clean" host rock sample. Despite this high fluid infiltration, alteration into Chl is quite low in these samples.

Ep displays a poikilistic texture with inclusions of Omp and Spn, and have a subhedral-anhedral form (fig. 22).

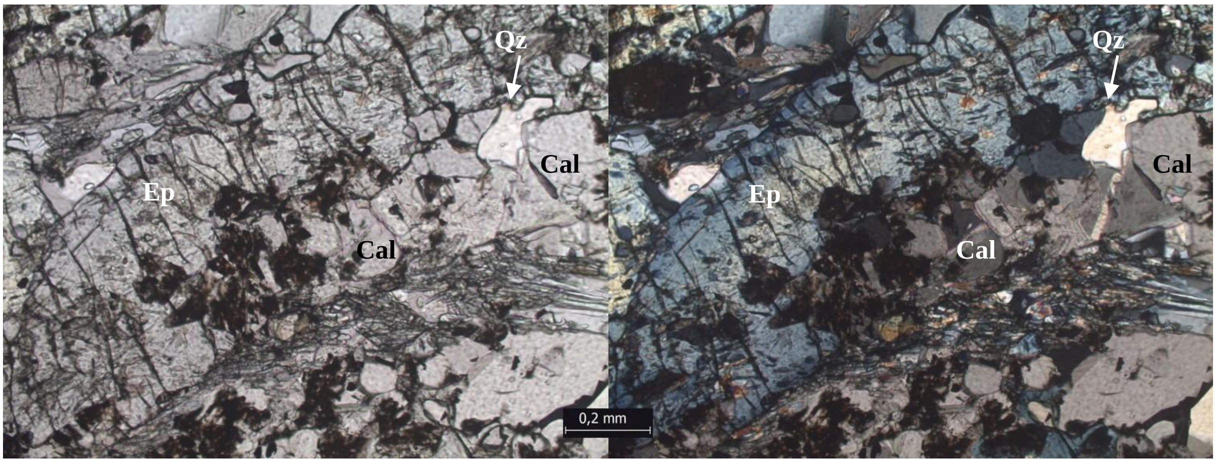

Fig. 22: Ep being altered into Cal and Qz. Late stage dolomitization of Cal is seen as "blurry" brown spots. PPL to the left, XPL to the right.

Wm occurs both as matrix-sized crystals as well as porphyroblasts (fig. 23A and B). The presence of Ep overgrowing the former location of the Wm porphyroblast in fig. 23C and D, indicates that the Wm porphyroblasts might have formed prior to the Ep, or that they were intergrown and therefore formed at the same time. Omp can be seen growing in the place where a Wm porphyroblast have been destroyed (fig. 23C and D).

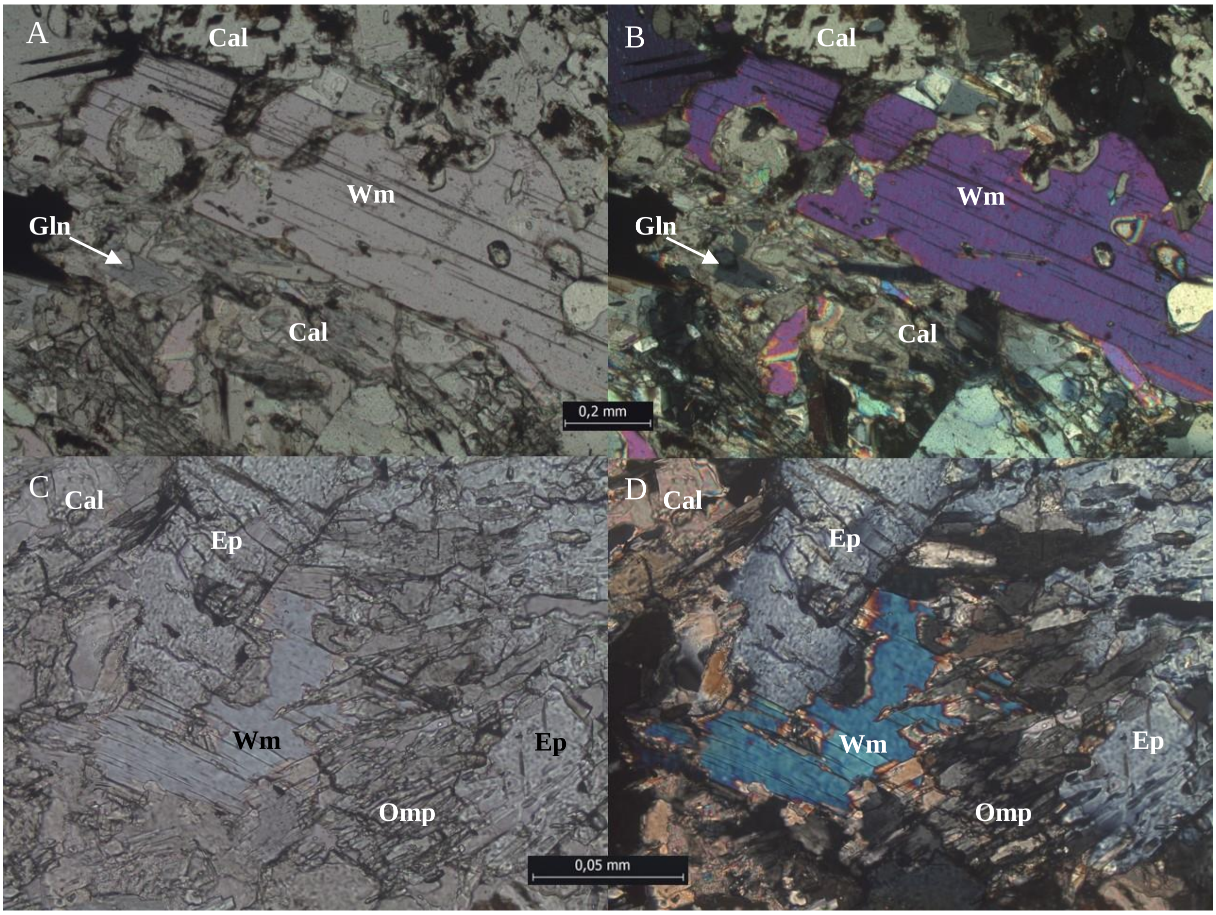

Fig. 23: A and B) Cal replacement of Wm porphyroblast, Omp and Gln. C and D) Anhedral Wm porphyroblast in association with an Ep porphyroblast, Chl, Cal, and matrix sized Omp. PPL to the left, XPL to the right. Note the difference in scale between upper and lower fig.

Cal is seen growing in the cracks of a porphyroblastic Amp (fig. 24), situated at the far end of the thin section, relative to the vein, which is a good example of how highly affected by fluids this host rock is.

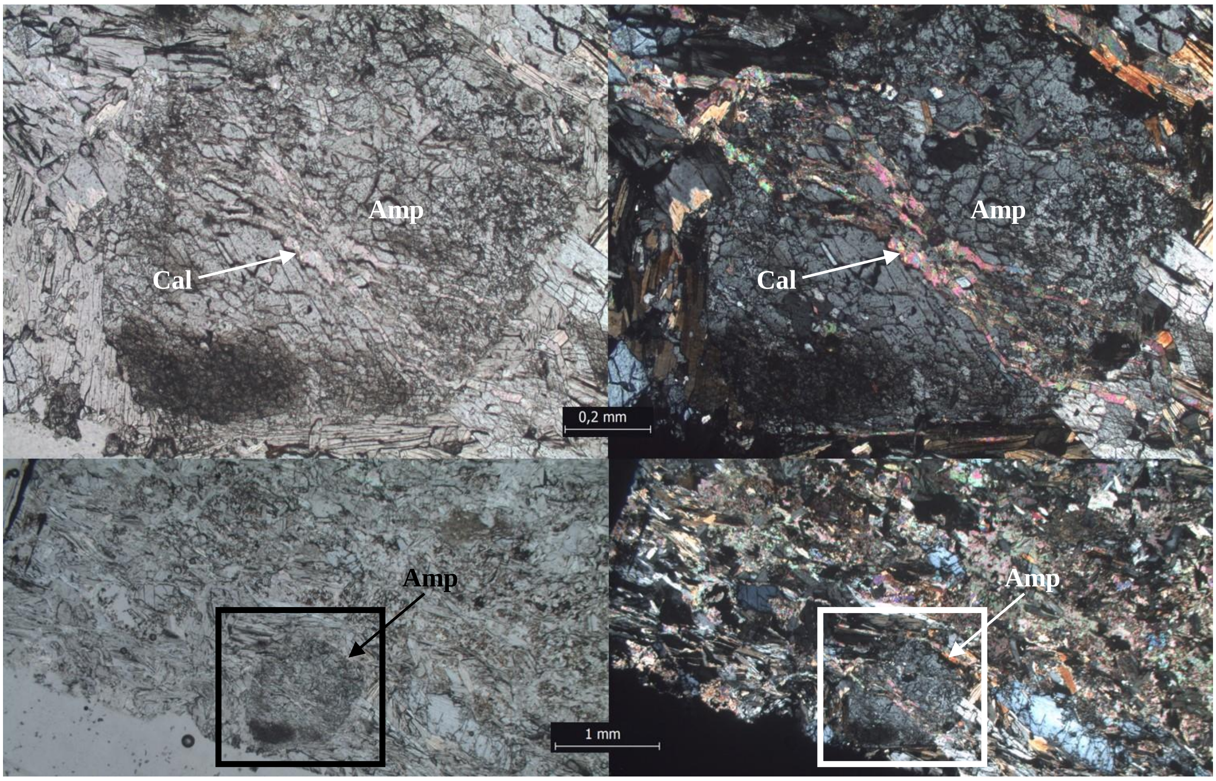

Fig. 24: Cal growing in cracks of porphyroblastic Amp. Left in PPL, right in XPL. Note the difference in scale between upper and lower fig., with the upper being a magnification of the same crystal as indicated by the square frame in the lower fig.

Most Grt poikiloblasts in the host rock are anhedral as they are highly altered into Cal and Qz, ± Chl (fig. 25), but within patches of Qz, smaller, euhedral Grt can be seen (fig.25). Gln in the host rock is almost solely found in association with Grt, as was described in sample SY-CM-01.

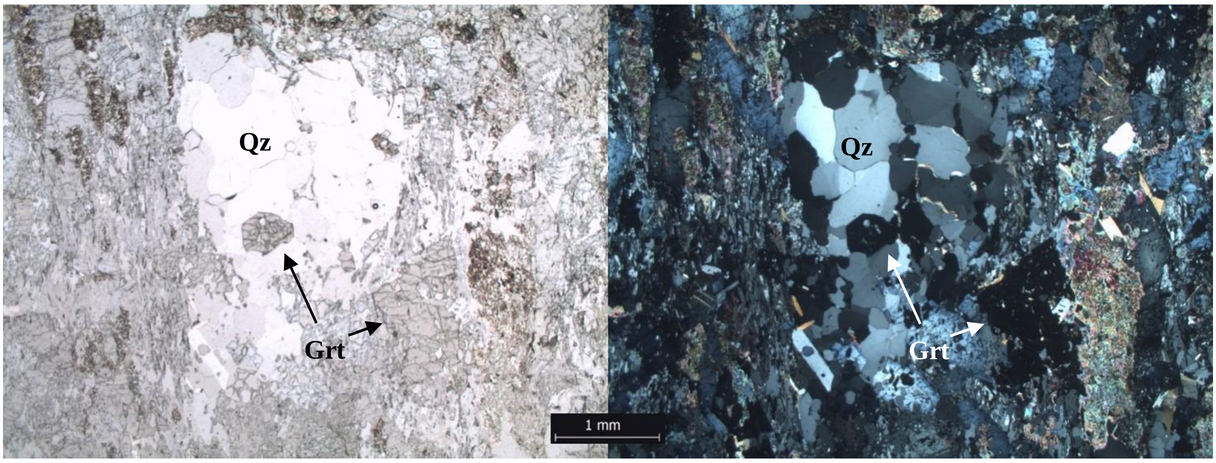

Fig. 25: Euhedral Grt protected from fluid alteration within a Qz cluster, with an unprotected, highly altered anhedral Grt to the right. PPL to the left, XPL to the right.

In the host rock the indications for deformation are seen as undulose extinction, recrystallization with Ostwald ripening and 120° triple junctions in places, as well as the matrix minerals aligning in a preferred orientation at an angle to the vein, as does some porphyroblasts.

Vein

The vein of this sample ranges in width from 1.5 to 4 mm. The minerals are white and translucent, and an orange tint can be seen on the weathered surfaces as well as on the fresh cut surface, thus this alteration is pervasive and not due to surface weathering (fig. 20). The orange tint is therefore interpreted as being from a post-metamorphic alteration of Cal into Dol (Schumacher *et al.*, 2008). This pervasive orange tint is not seen in the vein of sample SY-CM-01-green, nor in the SY-CM-03-green vein.

Indications of this vein opening while the rock had a brittle-ductile behaviour can be hinted from the foliation on either side being deflected into the vein.

Point counting of the vein reveals a very high modal abundance of Cal (81%, error 7.85, table 2) in this sample, while Qz makes up for 12% of the vein (error 6.5, table 2). The high modal abundance of Cal might be the reason for the orange colour from dolomitization being so clearly seen here, and not in the other vein samples containing a lower abundance of Cal (61% and 66%, error 4.88 and 4.74, tables 1 and 3), thus having less Cal that can react into Dol.

Minor amounts of Ep, Wm, Pl, Gln and Opq are present. Ep, Wm and Gln are relics from the host rock trapped in the vein, while Pl is considered a reaction product.

The size of the Cal crystals decreases towards the centre of the vein (fig. 26) with the larger crystals at the edges of the vein displaying undulose extinction. This decrease in crystal size towards the centre could be either from later crystallization or higher nucleation at the centre, or from recrystallization at the centre of the vein (fig. 27B) due to deformation strain. Some Cal crystals displays deformation twinning. Undulose extinction and recrystallization are seen in the Qz-crystals (fig. 27).

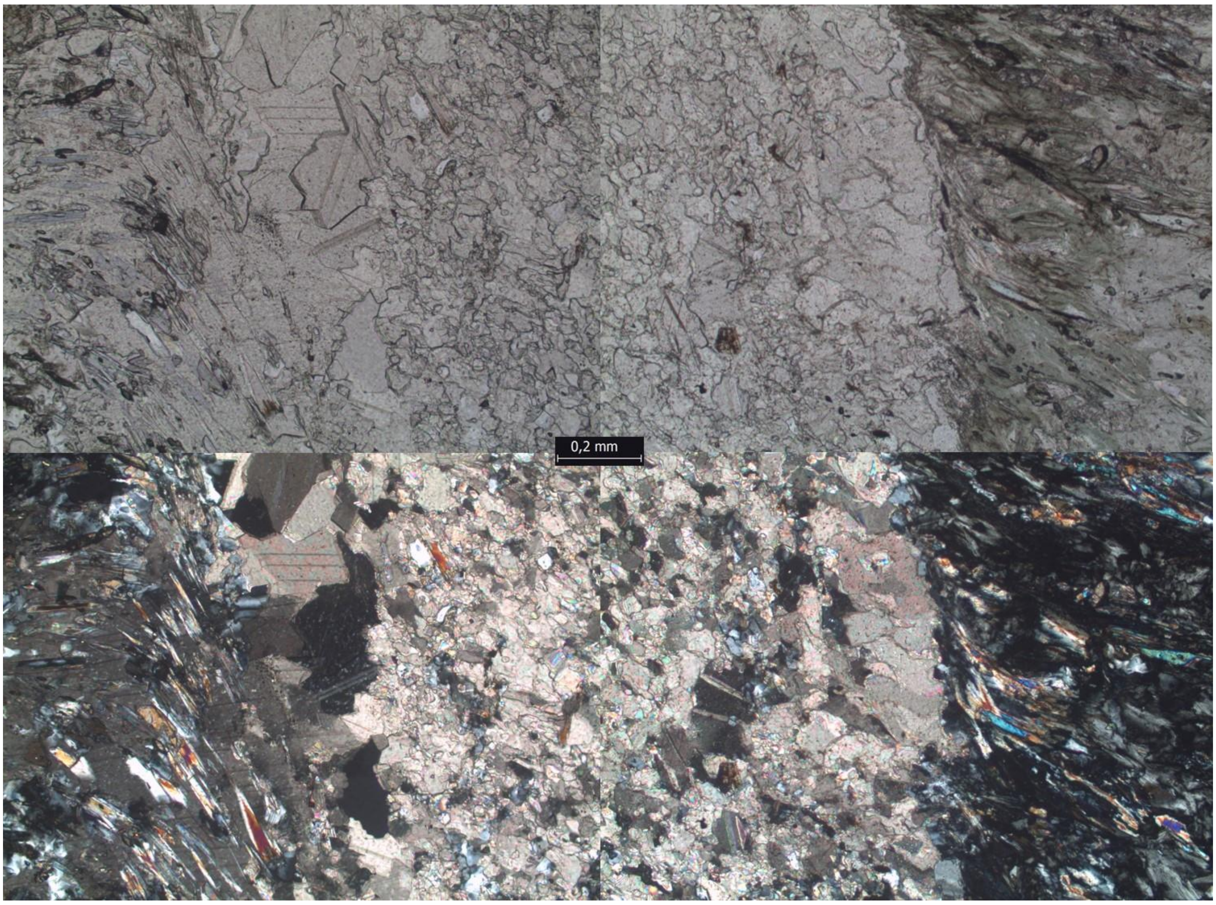

Fig. 26: Deflection of foliation into the vein indicating brittle-ductile deformation. Upper images in PPL, lower in XPL.

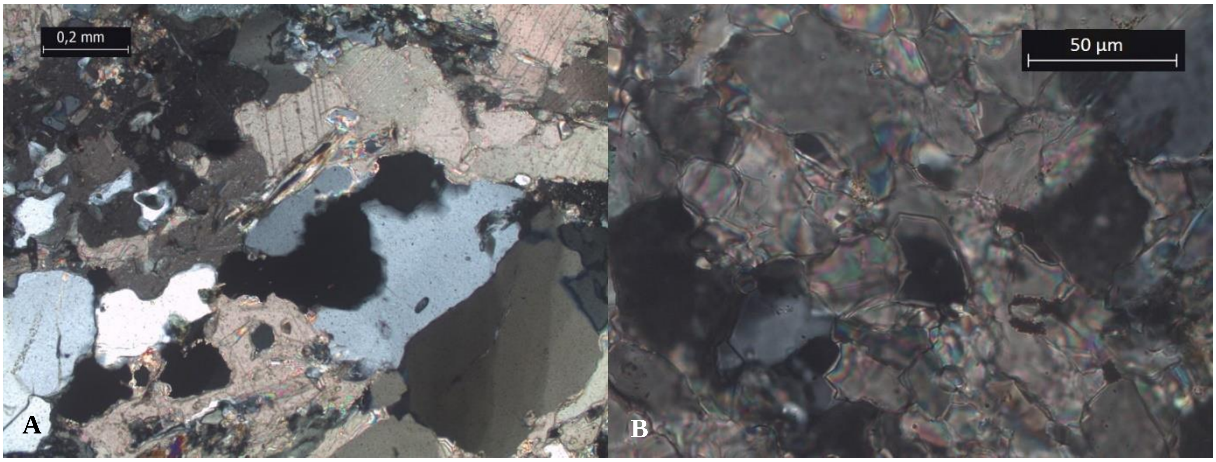

Fig. 27: A) GBM and undulose extinction in vein minerals. B) Recrystallization of minerals in the centre of the vein as seen by angles between the crystals. Both photos from sample SY-CM-03-02 and in XPL. Note the difference in scale.

Gln is reacting into Cal (fig. 28), and is only seen in the vein-halo transition, not in the more centred parts of the vein.

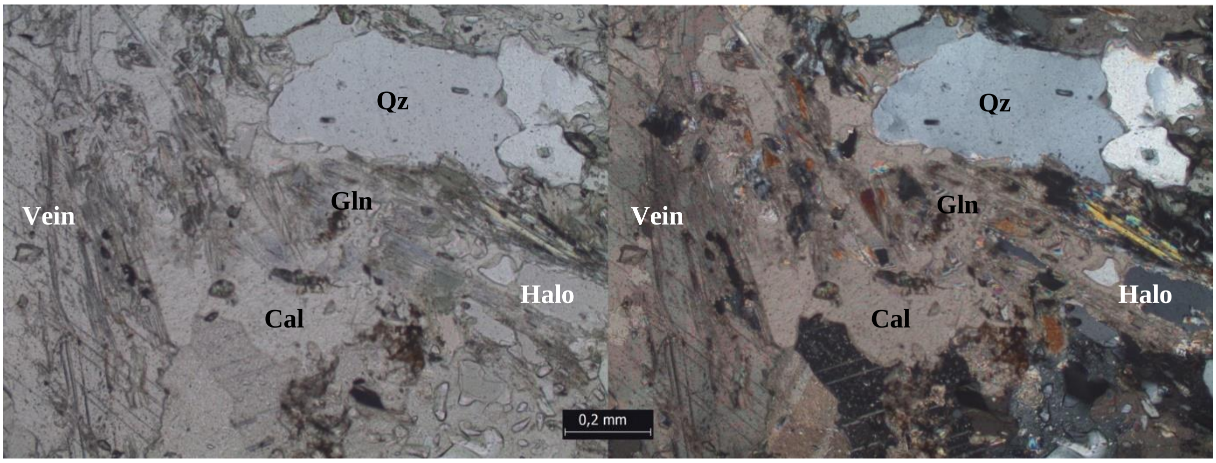

Fig. 28: Gln reacting into Cal in the vein-halo transition of sample SY-CM-03-02. PPL to the left, XPL to the right.

Ep and Wm display highly altered forms (reacting into Cal and Qz), as well as a very low abundance (tables 2 and 4). Pl is also of low abundance, but is considered a reaction product. Opq are focused at the edges of the vein.

The rock has been subjected to stress, which is apparent when considering the deflecting mineral grains in the halo flanking the vein (fig. 26). This confirms that the vein formed during brittle-ductile behaviour of the eclogite meta-basalt, providing a basis for determining the relative ages of the veins in the outcrop studied.

Reaction halo

The halo in this sample was in the field interpreted as being of blueschist facies due to the fine grained mineralogy containing Gln, yielding a distinct blue colour to the halo (fig. 20), and Ep (Philpotts & Ague, 2009; Winter, 2014). The width of each halo ranges from 3-10 mm. Both sides display this variety in width (fig. 20), indicating that the fluid infiltration into the host rock was approximately the same on both sides of the vein. The halo displays its bluest colour in the parts closest to the vein.

The orange alteration streaks are not as abundant in the halo as they are in the host rock (fig. 20). Some Wm porphyroblasts are present in the halo, but the abundance is lower, and the size smaller (0.5-2 mm in length and 0.25-0.5 mm in width), compared to those seen in the host rock. This indicates that the Wm porphyroblasts in the halo are remnants that are being altered. Gln might have a slight trend at orienting in the same manner as the metamorphic foliation, but since the crystals are small, quite scarce and/or highly altered it is hard to distinguish definitely.

The point counting of the halo reveals that the mineralogy is similar to that of the host rock, but with big differences in modal abundance (table 2). All comparisons here will be done to the summarized values of host rock in sample SY-CM-01-green, since this was the host rock least affected by fluid infiltration.

The mineral with the highest modal abundance in the halo is Cal, reaching a percentage of 23.2% (error 3.78, table 2), while the modal abundance of Chl, Omp, Gln, and Ep are quite similar (18.8% (3.49), 15.8% (3.26), 15.4% (3.23) and 13.2% (3.03) (error) respectively, table 2). Qz and Wm account for a few percent of the sample, while Grt and Spn only occur as minor phases.

Comparison between the summarized modes of the halo and the host rock (table 4) show decreases in several of the mineral modes; Omp (-28%), Wm (-9%), Grt (-8.2%) and Ep (-6.9%). Increased modal abundance is seen in Chl (+18.1), Cal (+18.1), Gln (+14.6) and Qz (+4.1%).

This implies that Omp, Wm, Grt, and Ep are replaced by Chl, Cal, and Gln in the halo. This is supported by the following textures:

1. Omp is replaced by Cal and Chl (fig. 29A and B)
2. Both porphyroblastic and matrix Wm are partly replaced by Cal and Chl (fig. 30C and D, and fig. 31A-D).
3. Grt porphyroblasts are partly replaced by Cal ± Qz ± Chl (fig. 31A-D).
4. Ep is replaced by Chl and Cal, ± Qz (fig. 29).

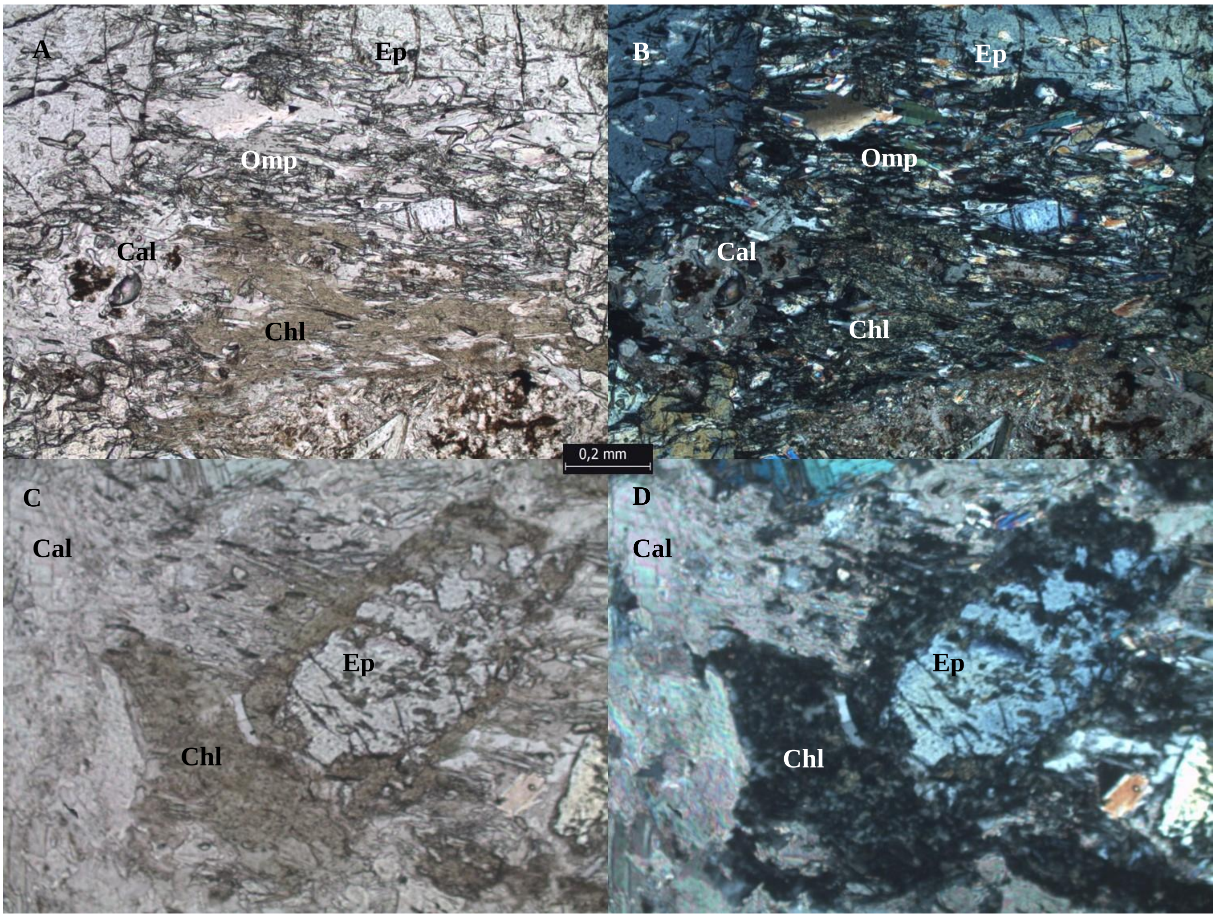

Fig. 29: A and B) Replacement of Omp by Chl and Cal. C and D) Anhedral Ep reacting into Chl and Cal close to the vein. Left side in PPL, right side in XPL.

Also:

Although Gln is showing an increase in modal abundance in the halo, in comparison to the host rock, Gln crystals can be seen altering into Cal and Chl (fig. 30A and B).

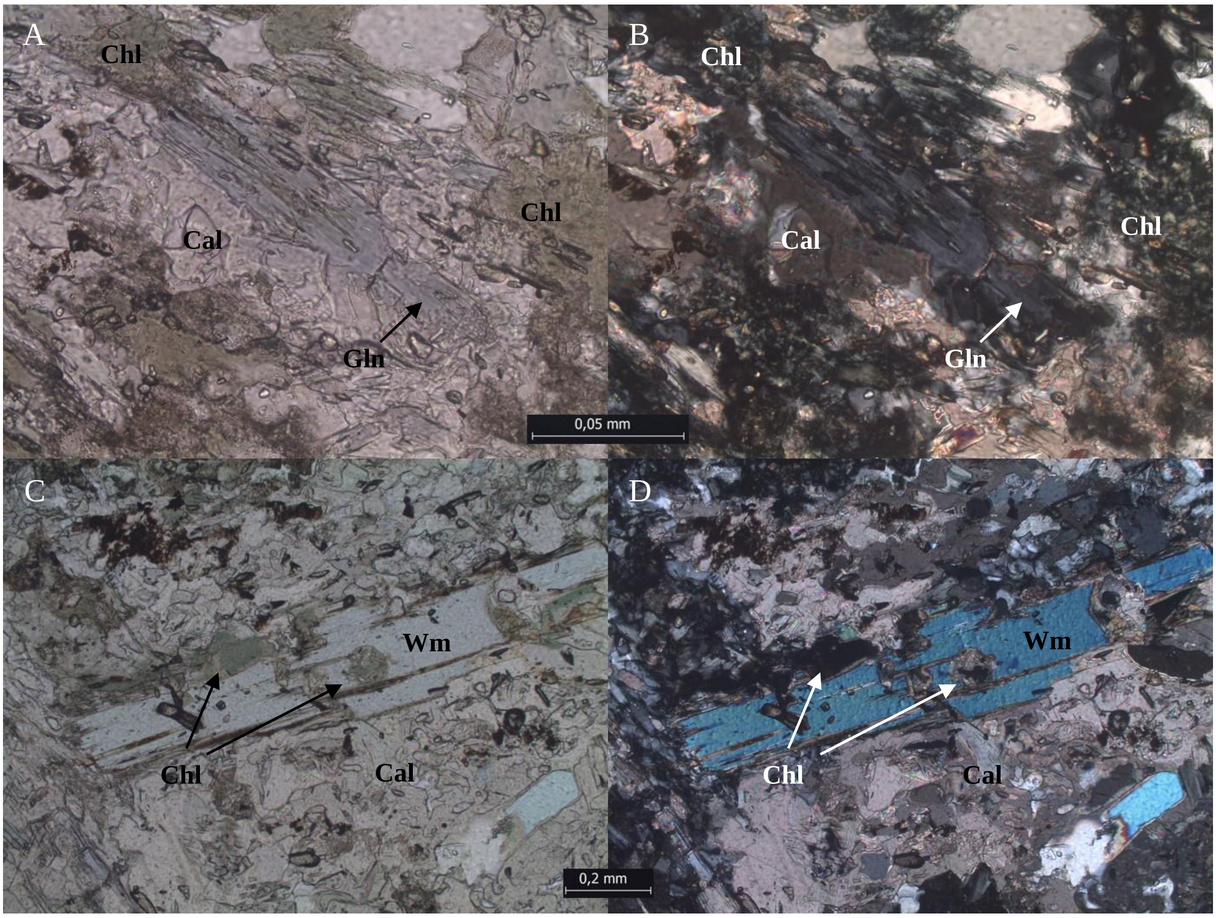

Fig. 30: A and B) A Gln crystal being altered into Cal and Chl. C and D) A Wm porphyroblast being altered into Cal and Chl. Left side in PPL, right side in XPL. Note the difference in scale.

Grt poikiloblasts are at places seen as highly altered, anhedral crystals (e.g. fig. 31A-D), although smaller sized, euhedral Grt can be seen in an area where fluids have infiltrated in higher quantities, causing an almost monomineralic area of Qz (fig. 31E and F). These small Grt might be euhedral either by them being protected from alteration by being enclosed in the Qz-patch, or from them being a new generation Grt of a different composition stable under the P-T conditions of the rock at the time of growth.

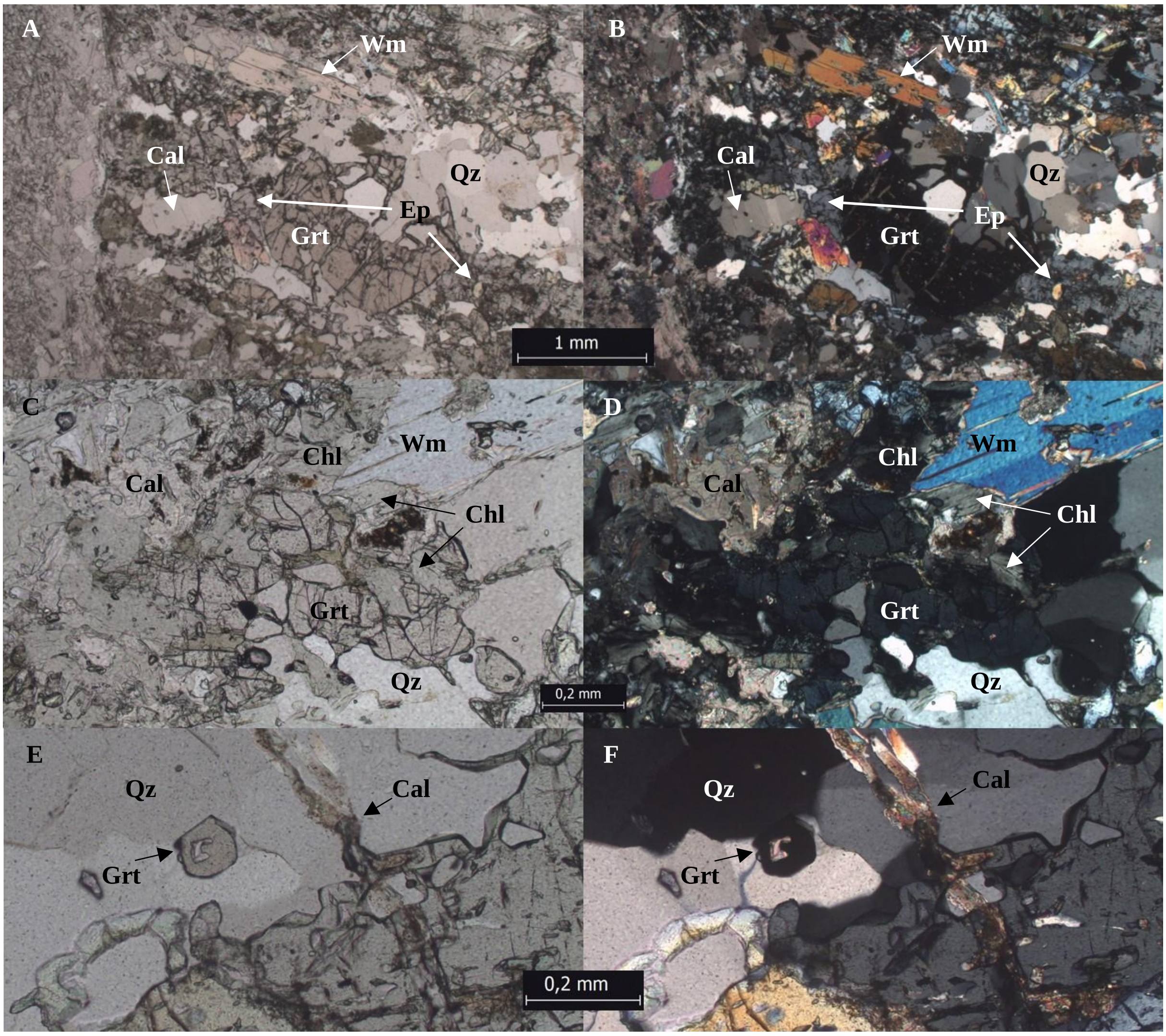

Fig. 31: A and B) Skeletal crystal of Grt in the halo with large Qz-crystal inclusions. An altering Wm porphyroblast is also seen. C and D) Anhedral Grt altering to Cal and Qz, as well as a Wm porphyroblast altering to Chl. E and F) Protected, or new generation of, Grt in an (almost) monomineralic patch of Qz. PPL to the left, XPL to the right. Note the difference in scale.

The reactions in the halo caused by fluid-rock interaction is also present in the host rock, albeit to a lesser extent. This implies that the halo is wider than the change in metamorphic facies, seen with the unaided eye, and has diffuse boundaries.

Deformation of the rock is evident by undulose extinction, GBM and Ostwald ripening of crystals (e.g. Qz, fig. 32), as well as most of the minerals displaying a preferred orientation parallel to the foliation. Cal can be seen as a thin film surrounding the Qz-crystals in fig. 32A.

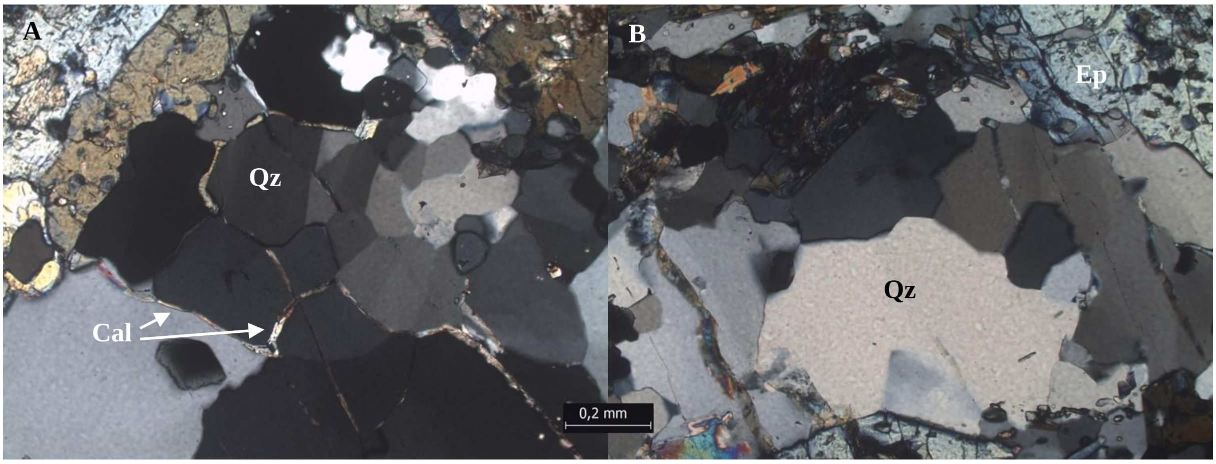

Fig. 32: GBM, undulose extinction and Ostwald ripening of Qz in the halo of SY-CM-03-02. Both fig. in XPL.

Overview of the thin sections of the sample provided in fig. 33.

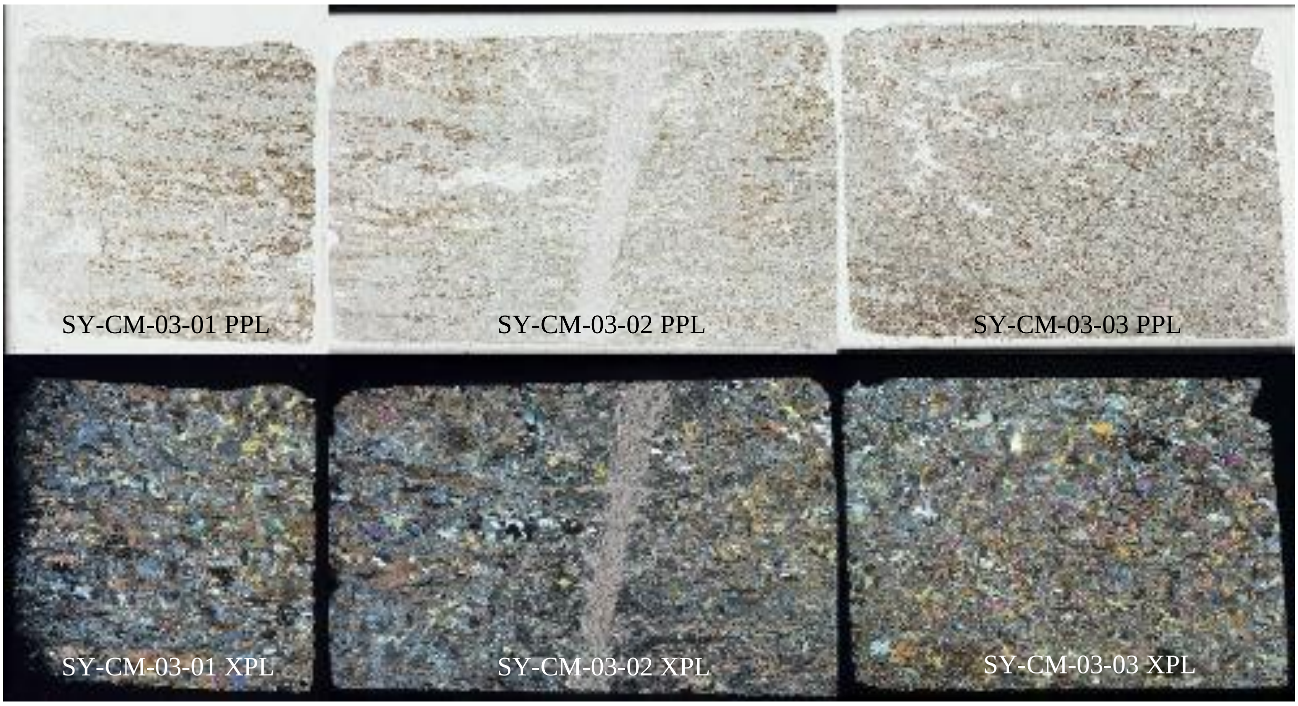

Fig. 33: Scanned images of thin section samples SY-CM-03-01/-02/-03. The 03-03 sample should probably be flipped upside-down to show the correct continuance of the 03-02 sample

Table 2: Modal abundance result from point counting of thin sections SY-CM-03-01, SY-CM-03-02, and SY-CM-03-03. Numbers in percent. For individual thin section counts see table 5B in appendix.

SY-CM-03-blue	**Host total**	error	**Halo total**	error	**Vein total**	error
Epidote	29.0	2.87	13.2	3.03	5.0	4.36
Omphacite	19.6	2.51	15.8	3.26	-	-
Glaucophane	1.1	0.66	15.4	3.23	-	-
Carbonates	27.5	2.82	23.2	3.78	81.0	7.85
Quartz	10.6	1.95	7.4	2.34	12.0	6.50
Garnet	1.6	0.79	0.2	0.40	-	-
White mica	8.2	1.74	5.2	1.99	2.0	2.80
Sphene	1.2	0.69	0.8	0.80	-	-
Chlorite	1.2	0.69	18.8	3.49	-	-
Opaque	-	-	-	-	-	-
Plagioclase	-	-	-	-	-	-
	1000p 100%		500p 100%		100p 100%	

SY-CM-03-green

Host rock

The host rock sample for SY-CM-03-green is the same as described for SY-CM-03-blue, since these samples were situated only cm´s apart in the outcrop (fig. 5 and 6).

The point counting of these samples reveal a host rock highly altered by fluid infiltration, as was the case in sample SY-CM-03-blue.

Omp is, as described in previous host rock samples, small, matrix sized crystals of high modal abundance that are aligned and defining the metamorphic foliation. Ep occurs as poikiloblasts with Omp inclusions, as in the other samples, and are subhedral-anhedral in shape due to alteration. Wm porphyroblasts are also subhedral-anhedral due to alteration (fig. 34).

Gln present in the host rock is only found in association with Grt (fig. 34), which, as aforementioned, could be from the Gln being shielded by the Grt. Gln and Grt are both reacting to form Cal, Qz and Chl (fig. 34). Opq in the host rock are only seen in association with Cal.

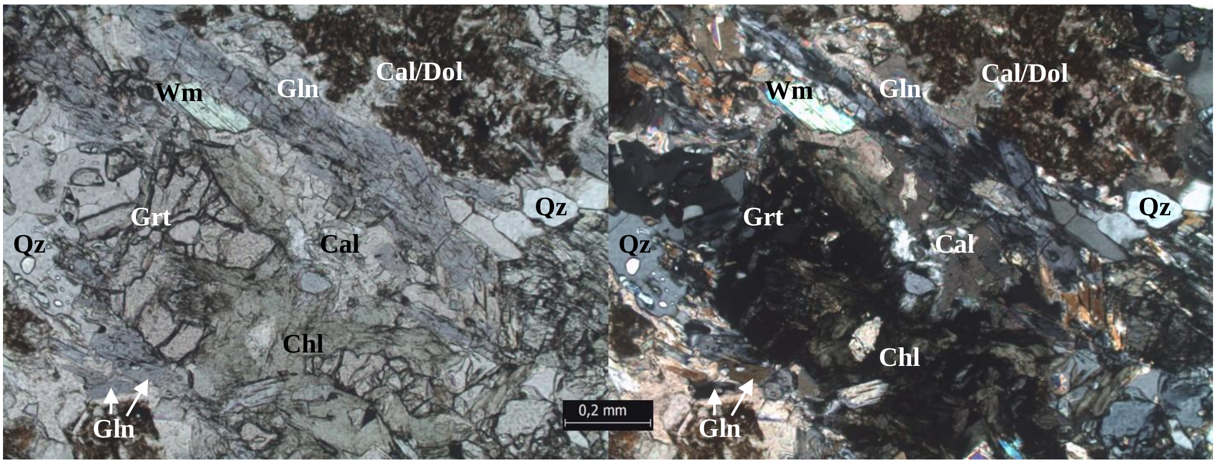

Fig. 34: Alteration of Gln, Wm and Grt. Left side PPL, right side XPL.

Qz crystals displays undulose extinction and GBM (as was the case in the other samples), indicating strain-induced alteration of the crystal lattices.

The dolomitization described in the other samples (Schumacher *et al.*, 2008), is present in these samples as well (brown "blurry" spots in fig. 34, and orange streaks in fig. 35).

Vein

The width of this vein cannot be determined since the rock at some time have split along the vein and one side halo and host rock are missing from the sample (fig. 5 and 35). The orange colour seen within the blueschist halo bearing vein is not present in this vein, although a slight hint of a yellowish tint can be seen in a few places.

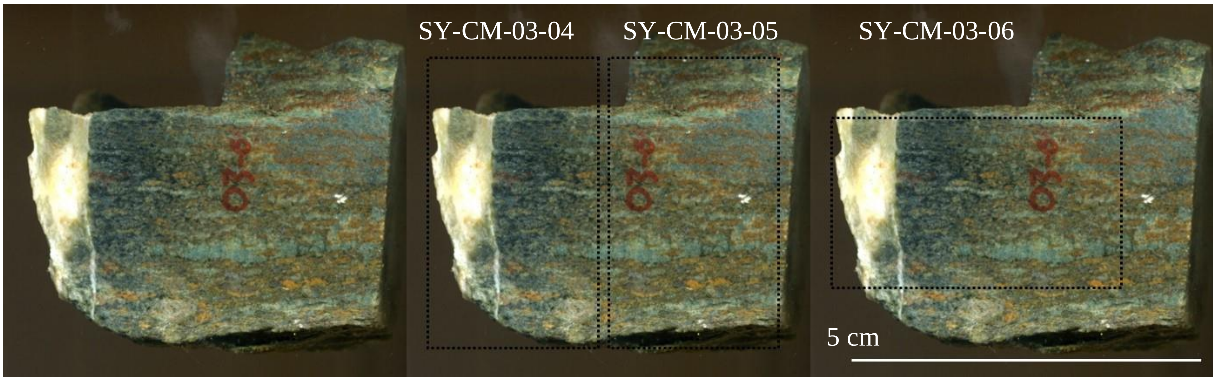

Fig. 35: Photo scanned cross-section of the SY-CM-03-green sample. Outlines showing the approximate position of thin sections SY-CM-03-04/-05/-06. All three images are the same.

The deflection of halo minerals into the vein in the halo-vein transition seen in sample SY-CM-03-blue is present in this sample as well (fig. 36), indicating the opening of this vein during P-T conditions causing brittle-ductile behaviour of the rock.

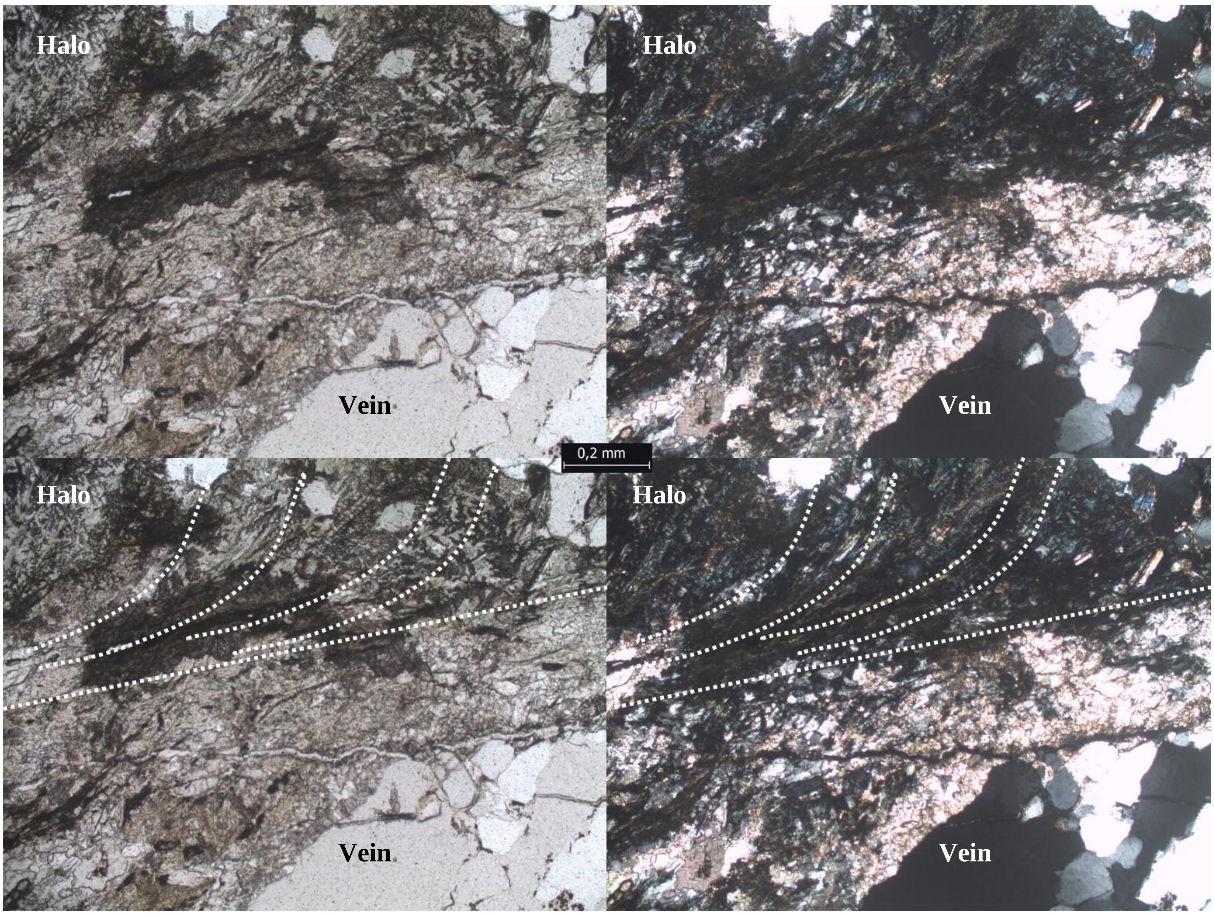

Fig. 36: Deflection of halo minerals into the vein indicating plastic deformation. Deflection indicated by curved dotted lines in lower fig. Straight line for separating the vein from the halo. Left side PPL, right side XPL.

The vein of this sample has quite a different mineralogy, and modal abundance, when compared to the other vein samples. Here the modal abundance of Ep, Pl, and even Chl is quite high (table 4). This is due to the vein being the result of (at least) two different individual veins merging together (fig. 5), and therefore "trapping" some of the host rock (now reset to the halo mineralogy) in between them, i.e. these are not true vein forming minerals, but host rock relics and reaction products.

The Spn is not as abundant in the vein as in the rest of the sample (halo and host rock, this goes for all the samples). There seems to be a new generation of really small Grt growing in an area of Qz, Cal and Pl at the edge of the vein, but it is hard to tell if this really is the case since these are located right at the edge of the thin section, causing some disturbance. A film of fine grained Cal can be seen at the edges of the larger Qz and Cal crystals (in the vein of sample SY-CM-03-blue this is seen as well, but is not to the same extent).

Qz seems to focus in clusters running along the strike of the vein in these samples. Undulose extinction, GBM, as well as some bent twinning in crystals of Cal (fig. 37) is seen in this sample, indicating that at least one deformation event has occurred after the crystallization the vein minerals.

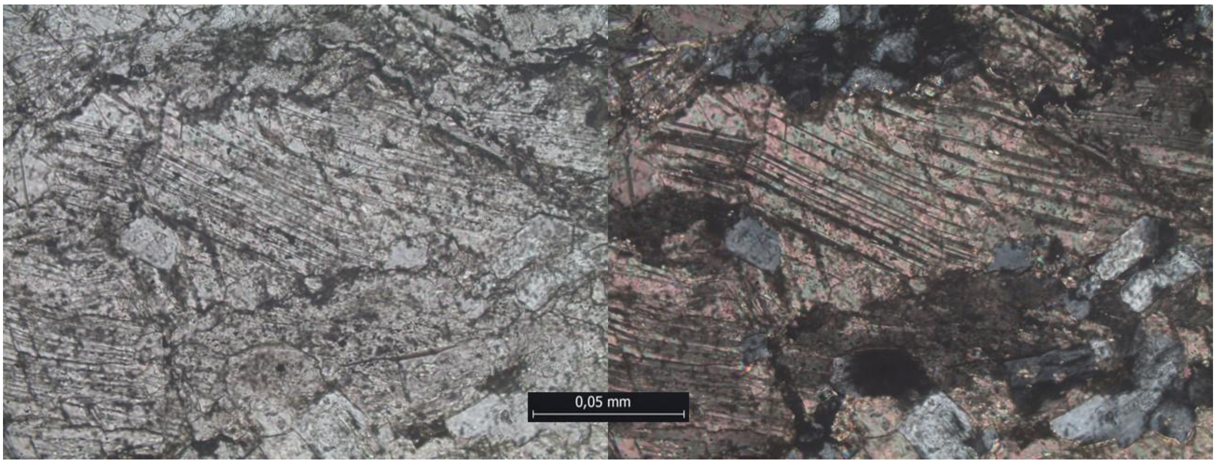

Fig. 37: Bent twinning in Cal indicating deformation of the crystal. PPL to the left, XPL to the right.

Deformation of the rock following crystallization of a (near to) monomineralic vein of Qz, running alongside one of the thin sections, is clear from the dislocation of said Qz-vein in the transition between the main vein and reaction halo (fig. 38). In the vein-halo transition, where the Qz-vein has been sheared, Cal is filling in the space (fig. 38), indicating that the deformation event causing the dislocation occurred when a CO_2-bearing fluid was present in the rock.

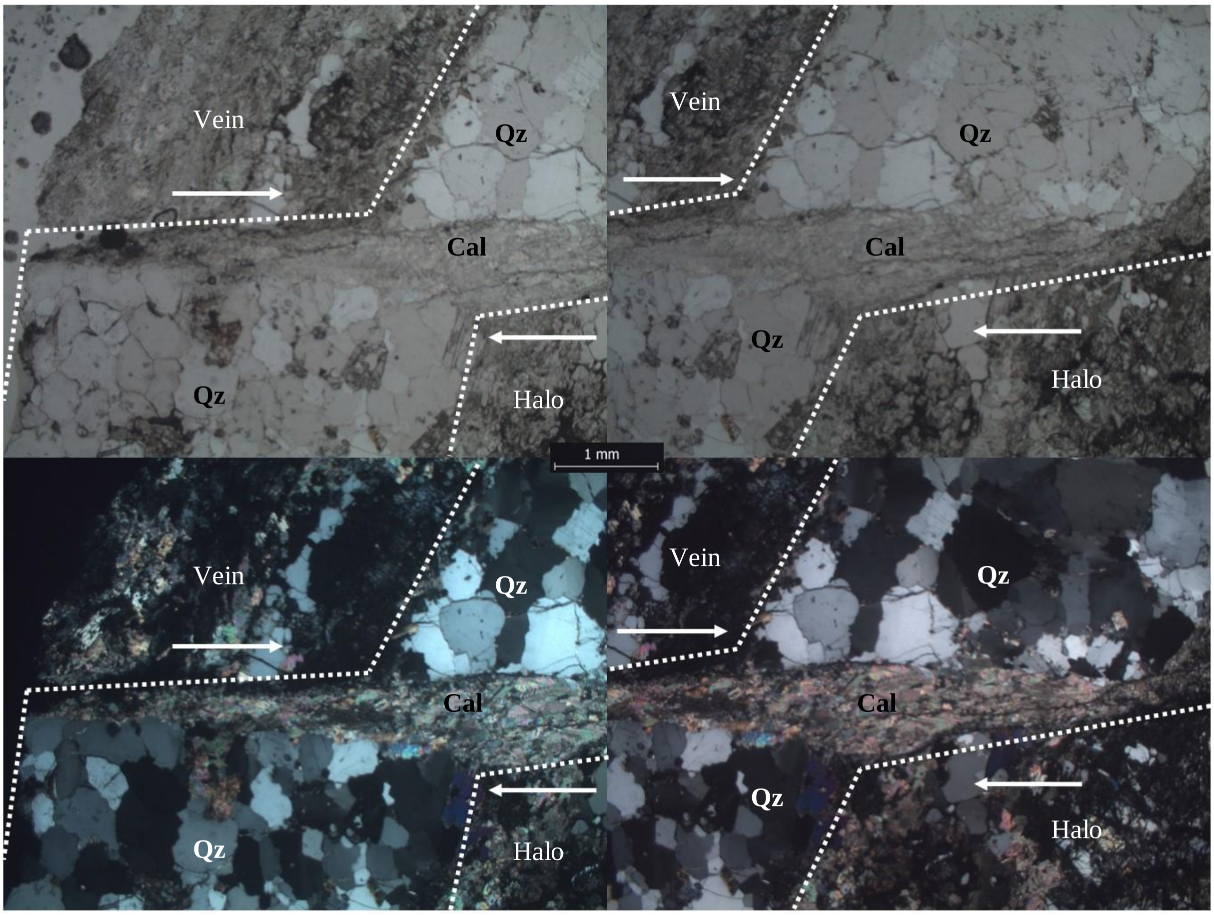

Fig. 38: Deformation shear sense in sample SY-CM-03-04 seen by the dislocation of a ~monomineralic vein of Qz. GBM and undulose extinction can be seen in the Qz. Upper in PPL, lower in XPL.

Reaction halo

The halo of this sample is interpreted as being of greenschist facies due to the high modal abundance of Chl, yielding a dark green colour to the halo (fig. 35), and the presence of Ep (Eskola, 1920), similar to the halo of sample SY-CM-01-green. Remnant Wm porphyroblasts are present, and the same Dol alteration streaks as described in the host rock can also be seen here (fig. 35). The orange alteration streaks are in the halo of a lower abundance, compared to that of the host rock (fig. 35), as was the case in the blueschist alteration halo.

Since the host rock of these samples are so highly altered from fluid infiltration, the comparison here will be done between the summarized values for the halo to the summarized values for the host rock of sample SY-CM-01-green, which is more representative for host rock.

The minerals with highest modal abundances from the point counting are Chl, Cal and Ep (33.8% (2.99), 21.8% (2.61), and 17.7% (2.41) (error) respectively, summarized values, table 3), supporting the greenschist facies classification (Eskola, 1920) made in the field. The halo also contains Qz (8.9% (1.8)) and Wm (7.4% (1.66)), as well as smaller amounts of Omp, Gln, Spn, and Pl.

Comparison between the summarized modes of the halo and host rock (table 4) shows decreases in most minerals, where the biggest decrease in modal abundance is seen in Omp (-39.3%), Grt (-8.4%) and Wm (-6.8%), and increase in Chl (+33.1%), Cal (+16.7%) and Qz (+5.6%) modes. Ep only shows a slight decrease when comparing the mode in the halo to the least fluid affected host rock, but when comparing the mode of Ep in the halo to the adjoining (fluid altered) host rock, a decrease of 12.3% is noted.

This implies that Omp, Grt, Wm and Ep are replaced by Chl, Cal and Qz in the halo, which is supported by the following textures:

1. Omp is almost completely altered into Chl (seen within the Ep crystal in fig. 39)
2. Grt poikiloblasts are replaced by Chl and Cal, ± Qz (fig. 40)
3. Both porphyroblastic and matrix Wm are being altered into Cal and Chl (fig. 39 and 41)
4. Ep poikiloblasts are in the halo replaced by Chl and Cal, ± Qz (fig. 39)

Also:

5. Gln is replaced by Chl and Cal (fig. 39)

The mineral modal abundance of this halo is quite different from the halo mineralogy in the near lying blueschist sample (SY-CM-03-blue, table 4, fig 6), but similar to the halo of the other greenschist sample (SY-CM-01-green), collected further away (table 4, fig. 6). The noticeable difference in comparing this halo to the other greenschist halo sample lies in the modal abundance of Qz (+7%, more in line with the near lying SY-CM-03-blue abundance), Chl (-10.8%) and Grt (-3.9%, only traces in this sample) (table 4).

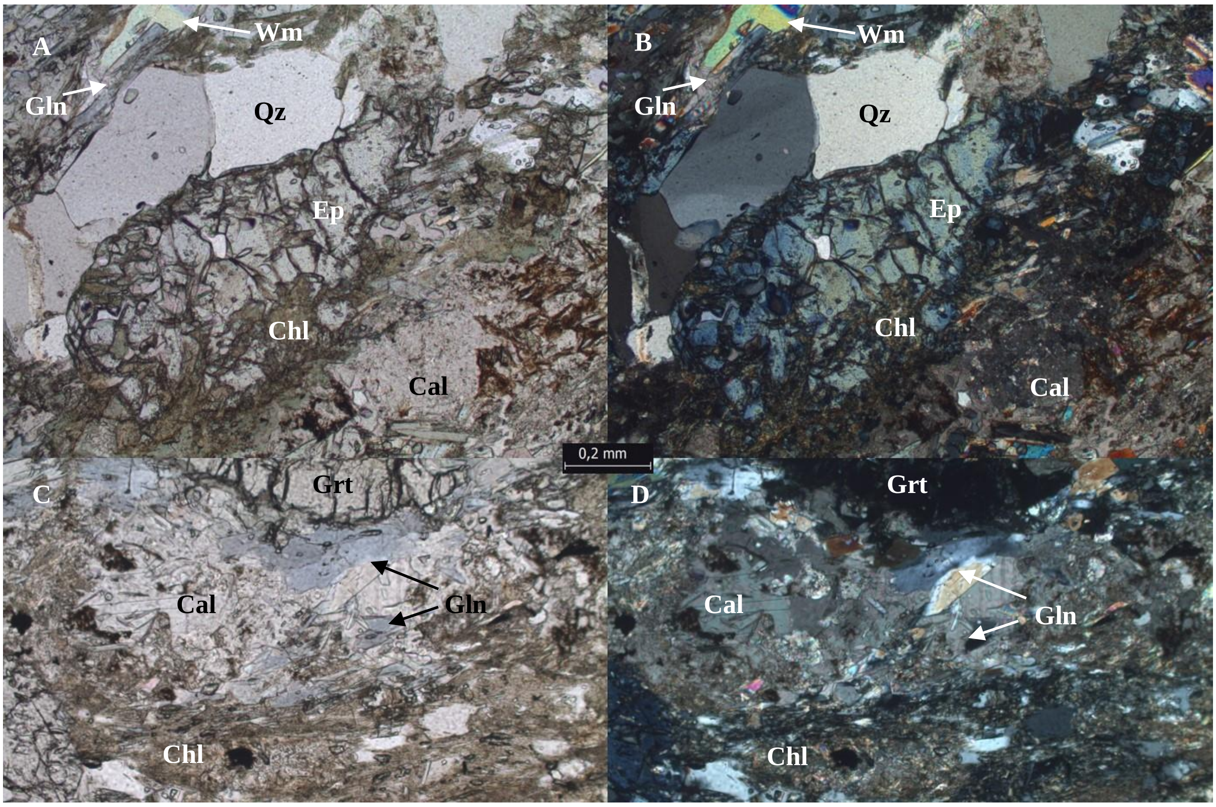

Fig. 39: A and B) Gln, Wm and Ep altering into Chl, Cal and Qz. C and D) Gln close to Grt and altering into Chl and Cal. Left side PPL, right side XPL.

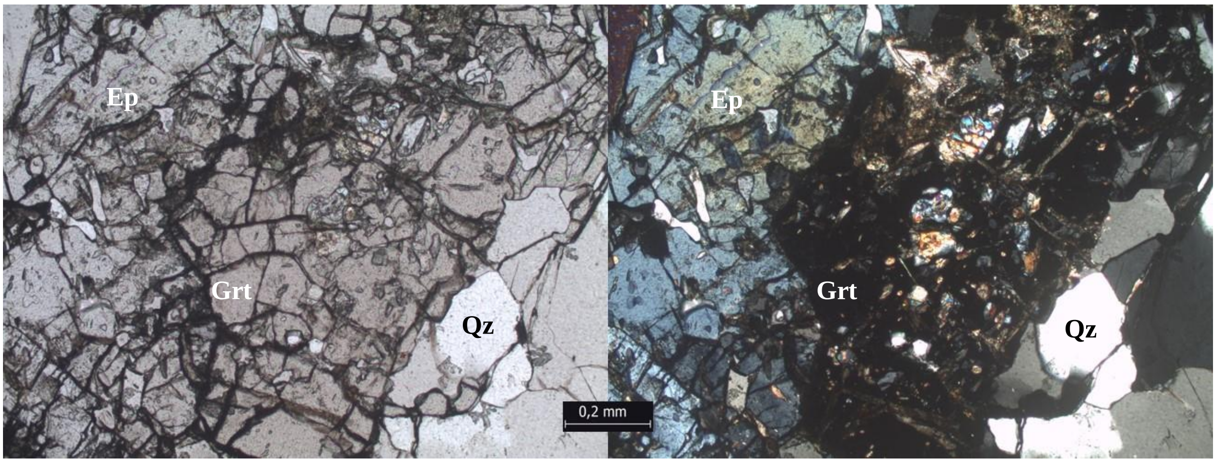

Fig. 40: Highly altered anhedral Grt. PPL to the left, XPL to the right.

Ep poikiloblasts have two preferred orientations, like in all other samples. Wm is present both as matrix-sized crystals oriented parallel to the foliation, as well as randomly oriented porphyroblasts, thus indicating two different generations of Wm, as in the other samples.

Some of the Ep and Wm porphyroblasts are intergrown, indicating that these porphyroblasts might have formed under the same P-T conditions (fig. 41).

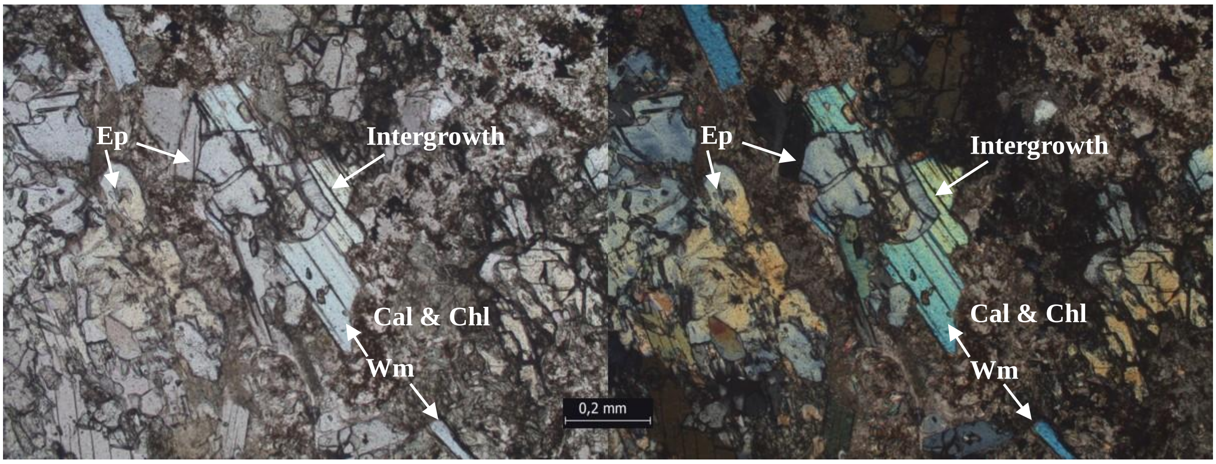

Fig. 41: Intergrown Ep and Wm porphyroblasts. Both minerals can be seen altering into Cal and Chl. The Dol alteration of Cal is also seen in these images. PPL to the left, XPL to the right.

The textures, alterations and preferred orientations of minerals are very similar here as in the other halo samples described above.

There is a vein of almost monomineralic Qz running along one side of all of sample SY-CM-03-04 (vein, rim and host rock) parallel to the foliation, as was mentioned in the vein description. Within this Qz-vein, pseudomorphs of Grt that have been completely altered into Cal and Qz (fig. 42) can be seen, as well as a thin film of Cal along Qtz grain boundaries.

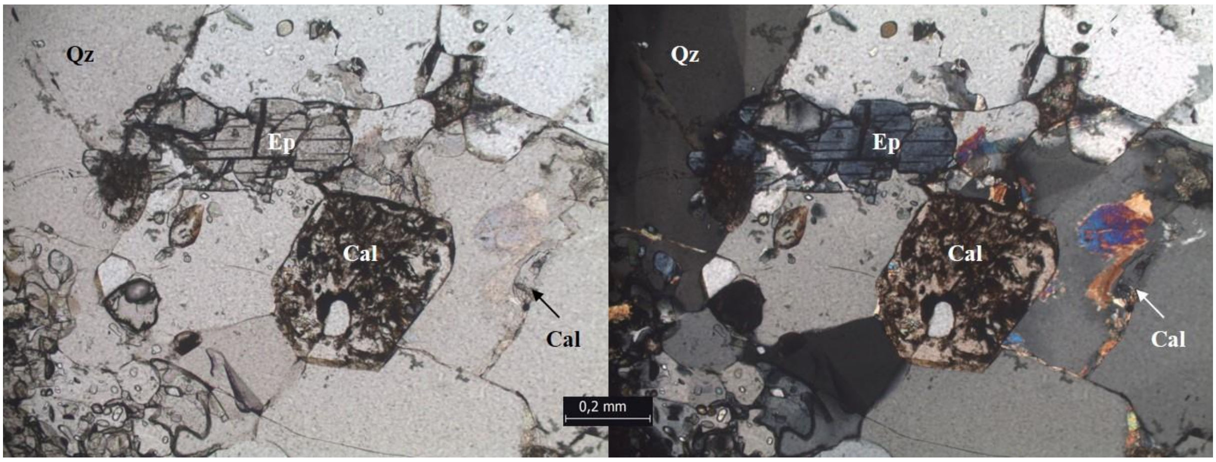

Fig. 42: Cal pseudomorph of Grt with Qz inclusion. PPL to the left, XPL to the right.

There are also some smaller sized, euhedral Grt present in this Qz-vein (see size difference of Grt pseudomorph in fig. 42 and euhedral Grts in fig. 43). These are believed to be either armoured by the surrounding Qz crystals, since they are all located within individual Qz crystals (fig. 43), and therefore not altering, or the result from growth of a new generation of Grt. If the latter is true, this indicates a state of equilibrium for Grt of the composition of the small ones, unlike the large poikiloblastic ones that are being replaced.

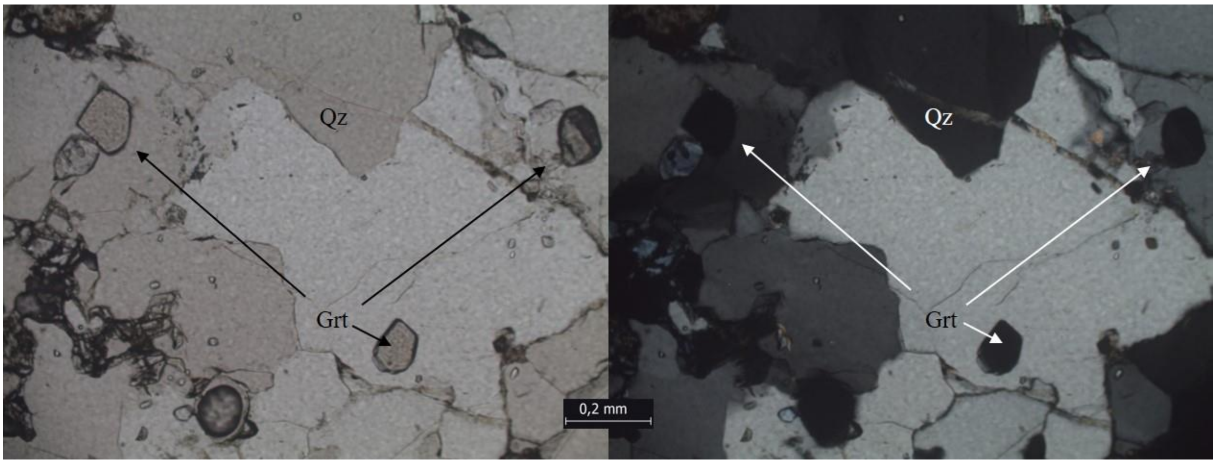

Fig. 43: Armoured, or growth of a new generation, Grt within a quartz vein running perpendicular to the main vein of the sample.

The Qz crystals of this vein displays undulose extinction and GBM, indicating deformation from strain in the crystal lattices.

Overview of the thin sections of the sample provided in fig. 44, where the aforementioned vein of Qz can be seen running along the lower side of thin section SY-CM-03-04.

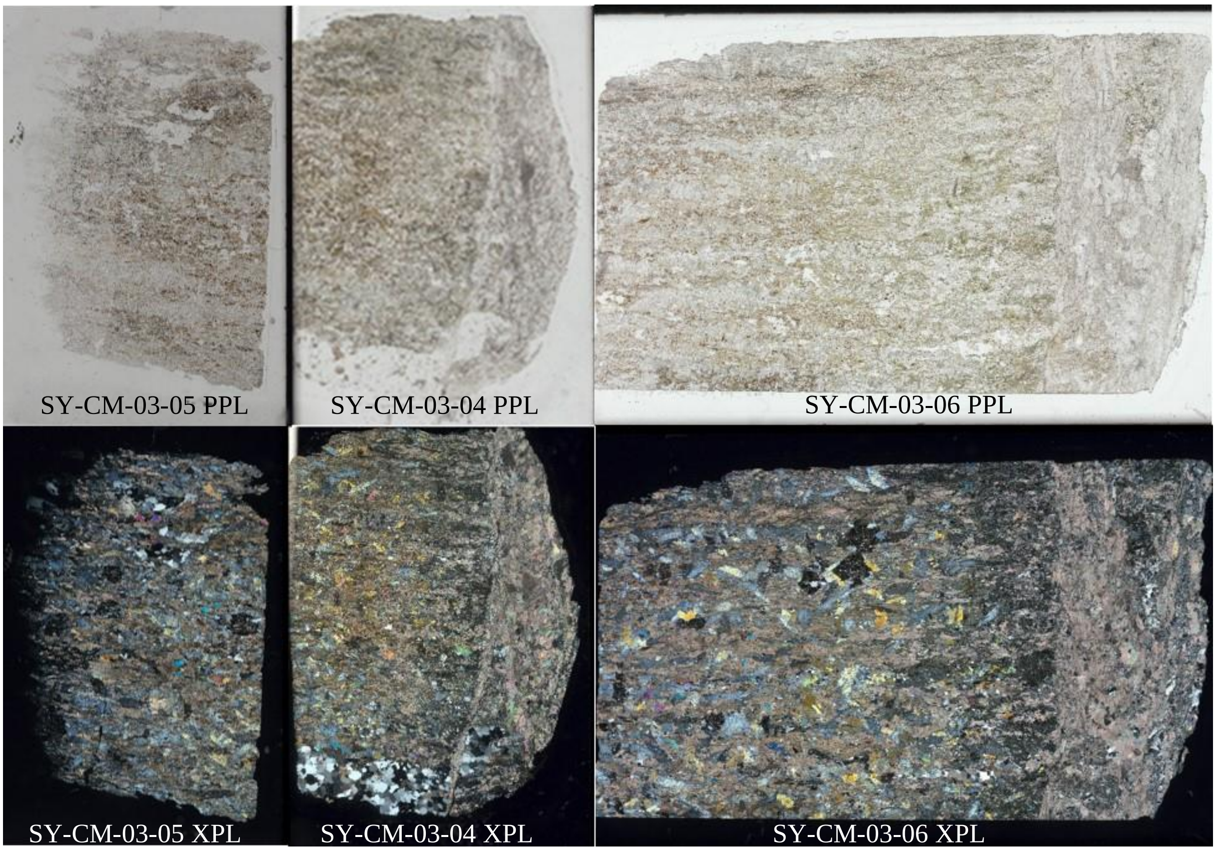

Fig. 44: Scanned images of thin section samples SY-CM-03-03/-04/-05

Table 3: Modal abundance result from point counting of thin sections SY-CM-03-04, SY-CM-03-05 and SY-CM-03-06. Numbers in percent. For individual thin section counts see table 5C in appendix.

SY-CM-03-green	**Host total**	error	**Halo total**	error	**Vein total**	error
Epidote	30.0	2.89	17.7	2.41	4.8	2.13
Omphacite	14.2	2.21	4.5	1.31	0.3	0.5
Glaucophane	1.7	0.82	2.2	0.93	-	-
Carbonates	22.6	2.65	21.8	2.61	66.0	4.74
Quartz	9.1	1.82	8.9	1.8	13.5	3.42
Garnet	1.0	0.63	-	-	-	-
White mica	7.5	1.67	7.4	1.66	0.5	0.71
Sphene	3.3	1.13	1.9	0.86	0.3	0.5
Chlorite	9.9	1.89	33.8	2.99	3.5	1.84
Opaque	0.7	0.53	-	-	-	-
Plagioclase	-	-	1.8	0.84	11.3	3.16
	1000p	100%	1000p	100%	400p	100%

Modal abundance

Table 4: Summarized modal abundance results retrieved from the point counting of the thin sections. Numbers in percent. For individual thin section counts and errors, see tables 5 A/B/C in appendix.

	SY-CM-01-green			**SY-CM-03-blue**			**SY-CM-03-green**		
	Host	Halo	Vein	Host	Halo	Vein	Host	Halo	Vein
Epidote	20.1	15.8	0.3	29.0	13.2	5.0	30.0	17.7	4.8
Omphacite	43.8	4.0	0.8	19.6	15.8	-	14.2	4.5	0.3
Glaucophane	0.8	0.6	-	1.1	15.4	-	1.7	2.2	-
Carbonates	5.1	18.4	61.0	27.5	23.2	81.0	22.6	21.8	66.0
Quartz	3.3	1.8	23.0	10.6	7.4	12.0	9.1	8.9	13.5
Garnet	8.4	3.9	-	1.6	0.2	-	1.0	-	-
White mica	14.2	7.8	1.0	8.2	5.2	2.0	7.5	7.4	0.5
Sphene	3.6	1.9	-	1.2	0.8	-	3.3	1.9	0.3
Chlorite	0.7	44.6	1.3	1.2	18.8	-	9.9	33.8	3.5
Opaque	-	1.4	4.0	-	-	-	0.7	-	-
Plagioclase	-	-	8.8	-	-	-	-	1.8	11.3

Discussion

The host rock of all samples is the same, i.e. eclogite facies meta-basalts. The differences that arises are due to differing extents of fluid rock interaction having affected the samples.

In all the samples, preferred orientation of the matrix minerals defines a pervasive metamorphic foliation. Most porphyroblasts display the same preferred orientation as the matrix minerals, although one generation Ep is aligning at an angle to the foliation and Wm porphyroblasts are randomly oriented.

The metamorphic foliation is present in both the host rock and the haloes of the samples. This implies that the mineralogy of the samples either developed before the foliation forming deformation event took place, or that the mineralogy in the haloes formed at a later stage and are mimicking an older preferred orientation already present in the host rock. Of these two scenarios, the latter seems more plausible since the alteration haloes are the result from fluid induced alteration of the host rock minerals, occurring after the opening of the veins.

When the result from the analyses made on the sampled veins, and their respective reaction haloes are put together, they reveal both the relative timing of the vein forming deformation events that the rock has been subjected to, as well as an insight in the composition of the fluids present.

A first vein forming event occurred while the rock volume was located under P-T conditions causing a brittle-ductile behaviour in the eclogitic rock, resulting in blueschist facies haloes to form alongside the veins. This was followed by a second vein forming event under greenschist facies conditions, retrogressing both the eclogite host rock in the haloes of the newly formed veins, as well as some of the older blueschist haloes, to a greenschist facies mineral assemblage. At the time of the greenschist overprint, the rocks acted in a brittle manner.

Modal data retrieved from point counting suggests that the reactions active in altering the vein selvage from an eclogite facies mineral assemblage, to that of a blueschist assemblage, are primarily the conversion of omphacite, epidote, white mica(s) and garnet into glaucophane, chlorite, calcite and quartz (table 4).

This interpretation is supported by the textural observations of epidote, omphacite, garnet and white mica(s) altering into chlorite, calcite and quartz (described under “SY-CM-03-blue reaction halo”).

When comparing the modal abundance of minerals between the summarized host rock percentages to that of the greenschist haloes, lining two of the sampled veins, the data suggests the breaking down of omphacite, epidote, garnet, and white mica(s), to produce chlorite and calcite, and in SY-CM-03-green, quartz as well.

This is supported by the reaction textures described in the “reaction halo” sections of the greenschist samples, where omphacite, epidote, garnet, and white mica(s) are all seen reacting to form chlorite, calcite and, all but white mica, quartz.

The reactions described for blueschist and greenschist samples are similar. What is causing the difference seen in facies of the halo is to what extent the reactions are occurring, and the amount of products minerals that are produced.

Relative timing of the vein forming events under differing P-T conditions can be inferred from the behaviour of the minerals alongside to the veins. In the two samples SY-CM-03, where one vein has a blueschist facies halo and the other a greenschist one (fig.6), the minerals in close proximity to the vein can be seen behaving in a ductile fashion, deflecting into the vein. This indicates that these two veins formed at approximately the same time, when the rock volume behaved in a brittle-ductile manner. The minerals in the greenschist facies halo of sample SY-CM-01 do not show any indication of such a deflection, which indicates that this vein opened as a result from brittle deformation under lower P-T conditions.

The difference in behaviour of the selvage minerals reveals the relative ages of the veins sampled, i.e. both veins in sample SY-CM-03 are of approximately the same age, despite the difference in facies seen in the haloes of the two, and pre-dates the vein of SY-CM-01. This is also implied, as was mentioned under “studied outcrop”, by the difference in strike of the veins sampled, where both SY-CM-03 samples strike sub-vertically, and SY-CM-01-green strikes at an angle to this (fig. 6). The difference in the strike of the veins is from the deformation events having different $\sigma 3$ (the direction of minimal stress, in which the vein opens). Put together, this indicates that there have been (at least) two individual vein forming events in the exhumation history of the eclogite rock volume.

The difference in metamorphic facies of, and modal abundance of minerals in, the haloes and veins of the samples are the last pieces in unravelling the history of the studied outcrop, for the purpose of this study.

The difference in metamorphic facies of the haloes indicates that the sample with the blueschist halo had already been sealed by the time of the greenschist overprint, or that it has been subjected to a fluid of a different composition (higher in CO_2), than the fluid affecting the samples with greenschist haloes. A fluid with a higher CO_2-content could have aided in the stabilisation of the blueschist facies minerals, even under greenschist facies conditions, as was described by Kleine *et al*. (2014, fig. 45). Since minerals in the blueschist halo can be seen reacting to greenschist facies minerals, the latter scenario with differing composition of the fluids is the more plausible of the two.

When comparing the modal abundance of chlorite and glaucophane in the two greenschist facies haloes, the older SY-CM-03-green, which opened during blueschist facies conditions, has a lower abundance of chlorite, and higher abundance of glaucophane than does the younger SY-CM-01-green (table 4). This difference in modal abundance supports the interpretation of the SY-CM-03 sample opening during blueschist facies conditions, and being reset to a greenschist facies assemblage during retrogression (fig. 39 in SY-CM-03-green “reaction halo”), while the SY-CM-01-green had yet to open at that time. Plagioclase is interpreted as being a reaction product under greenschist facies conditions, since it is only found in the greenschist halo-bearing veins.

Conclusions

There have been (at least) two individual vein forming events at different P-T conditions during the exhumation history of the eclogite facies meta-basaltic rocks studied. The fluids in these veins caused hydration and carbonation of the minerals in the selvages of the veins.

The first veining event took place under blueschist facies conditions, where the eclogite meta-basaltic rock had a brittle-ductile behaviour, causing alteration haloes with a blueschist facies mineralogy to form in the vein haloes (samples SY-CM-03-blue and –green). This was later followed by a vein forming event, occurring under P-T conditions resulting in a brittle behaviour of the eclogite host rock, yielding a greenschist facies overprint both in the eclogite rock haloes flanking the newly formed veins (sample SY-CM-01-green), and in some of the blueschist haloes already present at the time (sample SY-CM-03-green).

The metamorphic fluids in the veins shows indications of being of two different compositions, where one type fluid (higher in CO_2) acted as a stabilizer for blueschist facies minerals, while the other type fluid re-equilibrated the mineralogy of the vein selvages to that normally seen in meta-basaltic rocks under greenschist facies conditions.

A summary time line can be concluded:

1. Subduction of sedimentary protoliths.
2. Vein forming event at blueschist facies and exhumation to the lower crust in an extrusion wedge.
3. Vein forming event at greenschist facies conditions, overprinting blueschist haloes where the CO_2 of the fluid is too low to stabilise these, and exhumation to the surface by low angle normal faults.

The behaviour, reactions and facies seen in the minerals in the haloes studied indicates that both of the hypothesis presented at the beginning of this thesis is true, i.e. the rock has been subjected to two individual vein forming events at differing P-T conditions, as well as fluids of different compositions being active in altering/stabilizing the selvages of the veins under similar P-T conditions.

Future work to be done:

- A more in depth analysis to derive the composition of fluids that have been present in the veins studied.
- Electron microprobe for more accurate identification of mineral compositions, e.g. composition of centre/rim of garnets to show prograde/retrograde growth.
- Collect and analyse more samples at different veins to see if this result can be seen all through the area, e.g. is there a difference depending on vein size? Difference in what side of the large shear zone (with knockers) the vein is located? Could the fluid flow and/or fluid composition differ on either side? Is the fluid displaying an elevated X_{CO2} only a localized phenomena, or can it be found in other fluid conduits in the area?

Acknowledgement

I would like to thank my supervisor Professor Alasdair Skelton, not only for making this thesis possible, but for being a guiding light through the whole process. I would also wish to thank Professor Uwe Ring for his support during the field work in Syros, and Dr. Alexandre Peillod and Elin Tollefsen for their help during field work in Syros, as well as for their assistance in the lab. I would like to thank my daughter Idun for always picking me up whenever I feel overwhelmed while in pursuit of my bachelor's degree.

Finally, I am most grateful towards the Swedish school system in general, and Stockholm University and the Department of Geological Sciences in particular, for providing quality education available for everyone!

References

Altherr, R., Schliestedt, M., Okrusch, M., Seidel, E., Kreuzer, H., Harre, W., Lenz, H., Wendt, I., Wagner, G.A. (1979). Geochronology of High-Pressure Rocks on Sifnos (Cyclades, Greece). *Contributions to Mineralogy and Petrology*. 70 (3), 245-255.

Avigad, D., Garfunkel, Z. (1989). Low-angle faults above and below a blueschist belt—Tinos Island, Cyclades, Greece. *Terra Nova*. 1 (2), 182-187.

Barrientos, X., Selverstone, J. (1993). Infiltration vs. thermal overprinting of epidote blueschists, Ile de Groix, France. *Geology*. 21 (1), 69-72.

Behr, W.M., Kotowski, A.J., Ashley, K.T. (2018). Dehydration-induced rheological heterogeneity and the deep tremor source in warm subduction zones. *Geology*. 46 (5), 475-478.

Bons, P.D., Elburg, M.A., Gomez-Rivas, E. (2012). A review of the formation of tectonic veins and their microstructures. *Journal of Structural Geology*. 43, 33-62.

Breeding, C.M., Ague, J.J., Bröcker, M., Bolton, E.W. (2003). Blueschist preservation in a retrograded, high-pressure, low-temperature metamorphic terrane, Tinos, Greece: Implications for fluid flow paths in subduction zones. *G3, Geochemistry, Geophysics, Geosystems*. 4 (1), 9001, doi: 10.1029/2002GC000380, 1.

Bröcker, M. (1990). Blueschist-to-greenschist transition in metabasites from Tinos Island, Cyclades, Greece: Compositional control or fluid infiltration? *Lithos*. 25 (1-3), 25-39.

Cliff, R.A., Bond, C.E., Butler, R.W.H., Dixon, J.E. (2017). Geochronological challenges posed by continuously developing tectonometamorphic systems: insights from Rb–Sr mica ages from the Cycladic Blueschist Belt, Syros (Greece). *Journal of Metamorphic Geology*. 35 (2), 197-211.

Dürr, S., Altherr, R., Keller, J. (1978). The median Aegean crystalline belt: stratigraphy, structure, metamorphism, magmatism. In: Closs, H., Roeder, D., Schmidt, K.E *Alps, Apennines, Hellenides*. Stuttgart: Schweizerbart. 455-476.

Ernst, W.G. (2006). Preservation/exhumation of ultrahigh-pressure subduction complexes. *Lithos*. 92 (3-4), 321–335.

Eskola, P. (1915). On the Relations between the Chemical and Mineralogical Composition in the Metamorphic Rocks of the Orijärvi region. *Bulletin de la Commission Geologique de Finlande*. 44.

Eskola, P. (1920). The mineral facies of rocks. *Norsk Geologisk Tidsskrift*. 6, 143-194.

Etheridge, M.A., Vall, V.J., Vernon, R.H. (1983). The role of the fluid phase during regional metamorphism and deformation. *Journal of Metamorphic Geology*. 1 (3), 205-226.

Jolivet, L., Brun, J-P. (2008). Cenozoic geodynamic evolution of the Aegean. *International Journal of Earth Sciences*. 99 (1), 109-138.

Keiter, M., Piepjohn, K., Ballhaus, C., Lagos, M., Bode, M. (2004). Structural development of high-pressure metamorphic rocks on Syros island (Cyclades, Greece). *Journal of Structural Geology*. 26 (8), 1433-1445.

Kleine, B.I., Skelton, A.D.L., Huet, B., Pitcairn, I.K. (2014). Preservation of Blueschist-facies Minerals along a Shear Zone by Coupled Metasomatism and Fast-flowing CO2-bearing Fluids. *Journal of Petrology*. 1-35.

Laurent, V., Lanari, P., Naïr, I., Augier, R., Lahfid, A., Jolivet, L. (2018). Exhumation of eclogite and blueschist (Cyclades, Greece): Pressure–temperature evolution determined by thermobarometry and garnet equilibrium modelling. *Journal of Metamorphic Geology*. 36 (6), 769-798.

Maluski. H., Bonneau, M., Kienast, J. R. (1987). Dating the metamorphic events in the Cycladic area: $^{39}Ar/^{40}Ar$ data from metamorphic rocks of the island of Syros (Greece). *Bulletin de la Société Géologique de France*. 3 (5), 833-842.

Manea, V.C., Manea, M., Kostoglodov, V., Currie, C.A., Sewell, G. (2004). Thermal structure, coupling and metamorphism in the Mexican subduction zone beneath Guerrero. *Geophysical Journal International*. 158 (2), 775-784.

Matthews, A., Schliestedt, M. (1984). Evolution of the blueschist and greenschist facies rocks of Sifnos, Cyclades, Greece. A stable isotope study of subduction-related metamorphism. *Contributions to Mineralogy and Petrology*. 88 (1-2), 150-163.

Palin, R.M., White, R.W. (2016). Emergence of blueschists on Earth linked to secular changes in oceanic crust composition. *Nature Geoscience*. 9, 60-64.

Parra, T., Vidal, O., Jolivet, L. (2002). Relation between the intensity of deformation and retrogression in blueschist metapelites of Tinos Island (Greece) evidenced by chlorite–mica local equilibria. *Lithos*. 63 (1-2), 41–66.

Peillod, A., Ring, U., Glodny, J., Skelton, A. (2017). An Eocene/Oligocene blueschist-/greenschist facies P-T loop from the Cycladic Blueschist Unit on Naxos Island, Greece: Deformation-related re-equilibration vs. thermal relaxation. *Journal of Metamorphic Geology*. 35 (7), 805-830.

Peillod, A. (2018). *The metamorphic history of Naxos (central Cyclades, Greece). Deciphering the Oligocene and Miocene exhumation events.* (Doctoral thesis, Stockholm University, Stockholm).

Philippon, M., Brun, J-P., Gueydan, F. (2011). Tectonics of the Syros blueschists (Cyclades, Greece): From subduction to Aegean extension. *Tectonics*. 30 (4), TC4001, doi:10.1029/2010TC002810.

Philpotts, A.R., Ague, J.J. (2009). *Principles of Igneous and Metamorphic Petrology*. 2nd ed. Cambridge, U.K.: Cambridge University Press. 422-423.

Ring, U., Laws, S., Bernet, M. (1999). Structural analysis of a complex nappe sequence and late- orogenic basins from the Aegean Island of Samos, Greece. *Journal of Structural Geology*. 21, 1575-1601.

Ring, U., Layer, P.W. (2003). High-pressure metamorphism in the Aegean, easternMediterranean: Underplating and exhumation from the Late Cretaceous until the Miocene to Recent above the retreating Hellenic subduction zone. *Tectonics*. 22 (1022), doi: 10.1029/2001TC001350, 3.

Ring, U., Glodny, J. (2010). No need for lithospheric extension for exhuming (U)HP rocks by normal faulting. *Journal of the Geological Society*. 167 (2), 225-228.

Robertson, A. H. F., Clift, P. D., Degnan, P. J., Jones, G. (1991). Palaeogeographic and palaeotectonic evolution of the Eastern Mediterranean Neotethys. *Palaeogeography, Palaeoclimatology, Palaeoecology*. 87 (1-4), 289-343.

Schumacher, J.C., Brady, J.B., Cheney, J.T., Tonnsen, R.R. (2008). Glaucophane-bearing Marbles on Syros, Greece. *Journal of Petrology*. 49 (9), 1667–1686.

Schliestedt, M., Matthews, A. (1987). Transformation of blueschist to greenschist facies rocks as a consequence of fluid infiltration, Sifnos (Cyclades), Greece. *Contributions to Mineralogy and Petrology*. 97 (2), 237–250.

Tomaschek, F., Kennedy, A., Villa, I., Lagos, M., Ballhaus, C. (2003). Zircons from Syros, Cyclades, Greece-Recrystallization and Mobilization of Zircon During High-Pressure Metamorphism. *Journal of Petrology*. 44 (11), 1977-2002.

van der Plas, L., Tobi, A.C. (1965). A chart for judging the reliability of point counting results. *American Journal of Science*. 263 (1), 87-90.

Vitale Brovarone, A., Groppo, C., Hetényi, G., Compagnoni, R., Malavieille, J. (2011). Coexistence of lawsonite-bearing eclogite and blueschist: phase equilibria modelling of Alpine Corsica metabasalts and petrological evolution of subducting slabs. *Journal of Metamorphic Geology*. 29 (5), 583-600.

Whitney, D.L., Evans, B.W. (2010). Abbreviations for names of rock-forming minerals. *American Mineralogist*. 95, 185–187.

Winter, J.D. (2014). *Principles of Igneous and Metamorphic Petrology*. 2nd ed. Essex, U.K.: Pearson Education Limited. 563, 571.

Appendix

Mineral abbreviations

Omp:	omphacite	Dol:	dolomite
Gln:	glaucophane	Spn:	sphene (titanite)
Ep:	epidote	Opq:	opaque
Grt:	garnet	Zrn:	zircon
Wm:	white mica	Cpx:	clinopyroxene
Qz:	quartz	Pl:	plagioclase
Cal:	calcite	Chl:	chlorite
Jd:	jadeite	Amp:	amphibole

Point counting errors

Tables 5 A/B/C: Point counting results with points counted, percentages and estimated errors presented. A representing sample SY-CM-01-green, B sample SY-CM-03- blue, and C sample SY-CM-03- green. Errors were estimated using the method of van der Plas & Tobi (1965).

A:

	SY-CM-01-01		error	SY-CM-01-01 halo		error	SY-CM-01-01 vein		error	SY-CM-01-02		error	SY-CM-01-02 halo		error	SY-CM-01-02 vein		error
Ep	100p	20%	3.58	68p	13.6%	3.07	1p	0.5%	1.00	101p	20.2%	3.59	58p	19.3%	4.58	-		
Omp	247p	49.4%	4.47	17p	3.4%	1.62	-			191p	38.2%	4.35	15p	5%	2.52	3p	1.5%	1.72
Gln	5p	1%	0.89	5p	1%	0.89	-			3p	0.6%	0.69	-			-		
Cal ($CaCO_3$)	18p	3.6%	1.67	109p	21.8%	3.69	111p	55.5%	7.03	33p	6.6%	2.22	38p	12.7%	3.85	134p	67%	6.65
Qtz	5p	1%	0.89	5p	1%	0.89	53p	26.5%	6.24	28p	5.6%	2.06	9p	3%	1.97	38p	19%	5.58
Grt	54p	10.8%	2.78	14p	2.8%	1.48	-			30p	6%	2.12	17p	5.7%	2.68	-		
Wm	64p	12.8%	2.99	40p	8%	2.43	4p	2%	1.98	78p	15.6%	3.25	22p	7.3%	3.00	-		
Spn	7p	1.4%	1.05	-			-			29p	5.8%	2.09	15p	5%	2.52	-		
Chl	-			231p	46.2%	4.46	-			7p	1.4%	1.05	126p	42%	5.70	5p	2.5%	2.21
Opaque	-			11p	2.2%	1.31	9p	4.5%	2.93	-			-			7p	3.5%	2.60
Pl	-			-			22p	11%	4.42	-			-			13p	6.5%	3.49
Total	500p	100%		500p	100%		200p	100%		500p	100%		300p	100%		200p	100%	

B:

	SY-CM-03-01		error	SY-CM-03-02 halo		error	SY-CM-03-02 vein		error	SY-CM-03-03		error
Ep	136p	27.2%	3.98	66p	13.2%	3.03	5p	5%	4.36	154p	30.8%	4.13
Omp	96p	19.2%	3.52	79p	15.8%	3.26	-			100p	20.0%	3.58
Gln	5p	1%	0.89	77p	15.4%	3.23	-			6p	1.2%	0.97
Cal ($CaCO_3$)	143p	28.6%	4.04	116p	23.2%	3.78	81p	81%	7.85	132p	26.4%	3.94
Qtz	49p	9.8%	2.66	37p	7.4%	2.34	12p	12%	6.50	57p	11.4%	2.84
Grt	6p	1.2%	0.97	1p	0.2%	0.40	-			10p	2%	1.25
Wm	46p	9.2%	2.59	26p	5.2%	1.99	2p	2%	2.80	36p	7.2%	2.31
Spn	9p	1.8%	1.19	4p	0.8%	0.80	-			3p	0.6%	0.69
Chl	10p	2%	1.25	94p	18.8%	3.49	-			2p	0.4%	0.57
Opaque	-			-			-			-		
Pl	-			-			-			-		
Total	500p	100%		500p	100%		100p	100%		500p	100%	

C:

	SY-CM-03-04 halo		error	SY-CM-03-04 vein		error	SY-CM-03-05		error	SY-CM-03-06		error	SY-CM-03-06 halo		error	SY-CM-03-06 vein		error
Ep	79p	15.8%	3.26	16p	8%	3.84	141p	28.2%	4.03	159p	31.8%	4.17	98p	19.6%	3.55	3p	1.5%	1.72
Omp	27p	5.4%	2.02	1p	0.5%	1.00	84p	16.8%	3.34	58p	11.6%	2.86	18p	3.6%	1.67	-		
Gln	19p	3.8%	1.71	-			17p	3.4%	1.62	-			3p	0.6%	0.69	-		
Cal ($CaCO_3$)	116p	23.2%	3.78	135p	67.5%	6.62	131p	26.2%	3.93	95p	19%	3.51	102p	20.4%	3.60	129p	64.5%	6.77
Qtz	41p	8.2%	2.45	19p	9.5%	4.15	63p	12.6%	2.97	28p	5.6%	2.06	48p	9.6%	2.64	35p	17.5%	5.37
Grt	-			-			10p	2%	1.25	-			-			-		
Wm	44p	8.8%	2.53	1p	0.5%	1.00	38p	7.6%	2.37	37p	7.4%	2.34	30p	6%	2.12	1p	0.5%	1.00
Spn	6p	1.2%	0.97	-			6p	1.2%	0.97	27p	5.4%	2.02	13p	2.6%	1.42	1p	0.5%	1.00
Chl	162p	32.4%	4.19	-			10p	2%	1.25	89p	17.8%	3.42	176p	35.2%	4.27	14p	7%	3.61
Opaque	-			-			-			7p	1.4%	1.05	-			-		
Pl	6p	1.2%	0.97	28p	14%	4.91	-			-			12p	2.4%	1.37	17p	8.5%	3.94
Total	500p	100%		200p	100%		500p	100%		500p	100%		500p	100%		200p	100%	

52